Journal of Advanced Ceramics
2022, **11**(9): 1343–1374
https://doi.org/10.1007/s40145-022-0611-5
ISSN 2226-4108
CN 10-1154/TQ

Review

Long-term ceramic matrix composite for aeroengine

Chaokun SONG, Fang YE*, Laifei CHENG*, Yongsheng LIU, Qing ZHANG*

Science and Technology on Thermostructure Composite Materials Laboratory, Northwestern Polytechnical University, Xi'an 710072, China

Received: March 3, 2022; Revised: May 1, 2022; Accepted: May 7, 2022

Abstract: Three strategies were proposed to prolong the service life of continuous fiber-reinforced silicon carbide ceramic matrix composite (CMC-SiC), which served as thermal-structure components of aeroengine at thermo-mechanical-oxygenic coupling environment. As for some thermal-structure components with low working stress, improving the degree of densification was crucial to prolong the service life, and the related process approaches were recited. If the thermal-structure components worked under moderate stress, the matrix cracking stress (σ_{mc}) should be improved as far as possible. The fiber preform architecture, interface shear strength, residual thermal stress, and matrix strengthening were associated with σ_{mc} in this review. Introducing self-healing components was quite significant with the appearance of matrix microcracks when CMC-SiC worked at more severe environment for hundreds of hours. The damage can be sealed by glass phase originating from the reaction between self-healing components and oxygen. The effective self-healing temperature range of different self-healing components was first summarized and distinguished. The structure, composition, and preparation process of CMC-SiC should be systematically designed and optimized to achieve long duration target.

Keywords: high degree of densification; matrix cracking stress; self-healing; duration; silicon carbide ceramic matrix composite (CMC-SiC)

1 Introduction

Owing to the excellent specific modulus and strength, and low density and non-brittle fracture behavior [1], silicon carbide ceramic matrix composite (CMC-SiC) has more and more extensive applications in high thrust-to-weight ratio aeroengine [2,3] (turbine shroud [4], exhaust nozzle [5], combustion chamber, turbine guide vane, turbine blade, etc. [6–9]). The thermo-mechanical-oxygenic coupling service environment puts forward higher requirements on CMC-SiC. The corrosion (heat corrosion and water corrosion) and oxidation are two serious problems faced by long-term CMC-SiC in harsh service environment. The environment barrier coatings (EBCs) have been widely applied to improve the corrosion resistance property [10–14]. This issue has been studied by a lot of literatures, and it is not further discussed in this review. If the interphase and fiber are oxidized, the mechanical property would decrease rapidly, and the CMC-SiC would fail prematurely [5,15–17]. Enhancing the oxidation resistance property to prolong the service life is the most urgent problem for

* Corresponding authors.
E-mail: F. Ye, yefang511@nwpu.edu.cn;
L. Cheng, chenglf@nwpu.edu.cn;
Q. Zhang, zhangqing@nwpu.edu.cn

the development of CMC-SiC.

Chemical vapor infiltration (CVI), precursor infiltration pyrolysis (PIP), and reactive melt infiltration (RMI) are three common methods to fabricate CMC-SiC. The open porosity of CMC-SiC via CVI is about 10%–15% [18,19] because the bottleneck effect exists in CVI process. Resulting from the volume shrinkage and gas releasing when the organic precursor transforms to inorganic ceramic [20], the CMC-SiC via PIP always contains 10% open pores. Though volume expansion is about 42% owing to the reaction between silicon and carbon during the RMI process (the molar volumes of C and SiC are 8.76 and 12.72 cm^3/mol, respectively [21]), the pores in porous carbon are difficult to be fully filled by the RMI SiC matrix. The open porosity of CMC-SiC via the RMI is about 2%–5% [22]. The holes in composites resulting from the preparation process provide diffusion pathway for oxygen. The interphase and fiber are going to be oxidized when CMC-SiC serves at high-temperature and oxidization environment [23]. As for C/SiC composite, the matrix microcracks come into being due to different coefficients of thermal expansion (CTEs) between carbon fiber and SiC matrix when the temperature decreases from preparation temperature to room temperature [24]. The matrix microcracks further provide diffusion pathway for oxygen, and the mechanical properties rapidly reduce when the service temperature is below preparation temperature. In addition to above two kinds of defects, the matrix microcracks also initiate when CMC-SiC is loaded above the matrix cracking stress (σ_{mc}) according to the stress–strain curve (Fig. 1) [19,25–27]. It promotes the interphase and fiber to react quickly with oxygen at high temperatures [17]. The service life of CMC-SiC is significantly decreased. To realize the wide application of CMC-SiC in the field of aerospace, effective measures must be taken to prolong the duration [15].

As shown in Fig. 2, there are three strategies to solve the above problems. For some thermal-structure components, like turbine shroud, the service condition is not too severe. The working stress is relatively low and located at linear segment of the stress–strain curve. It means that the cracks would not initiate when CMC-SiC is loaded. High degree of densification is the most urgent requirement for long-term CMC-SiC. The dense oxide scale generated on the surface can effectively impede the diffusion of oxygen and protect the inner material from oxidation. The oxidation would only occur at the surface of CMC-SiC. Related preparation techniques should be employed to fabricate the CMC-SiC with high density. As for exhaust nozzle and combustion chamber, the working stress is moderate. Increasing σ_{mc} of CMC-SiC is the key measure to prolong the duration. If the σ_{mc} is above working stress, the damage would not be formed, and the service property is improved. The fiber preform structure, interface shear strength, CTE match between fiber and matrix, and matrix strengthening need to be properly designed and adjusted to improve the σ_{mc}. When CMC-SiC components serve in medium stress for hundreds or thousands of hours, such as turbine guide vane and turbine blade, the matrix microcracks would inevitably generate. Introduction self-healing component is an effective method to enhance the environment performance of CMC-SiC [15,28]. On the one hand, the microcracks could be healed by the viscous flowing of glass phase (self-healing phase), which is derived from the oxidation of self-healing component. On the other hand, the oxidation process is accompanied by volume expansion. The cracks are closed

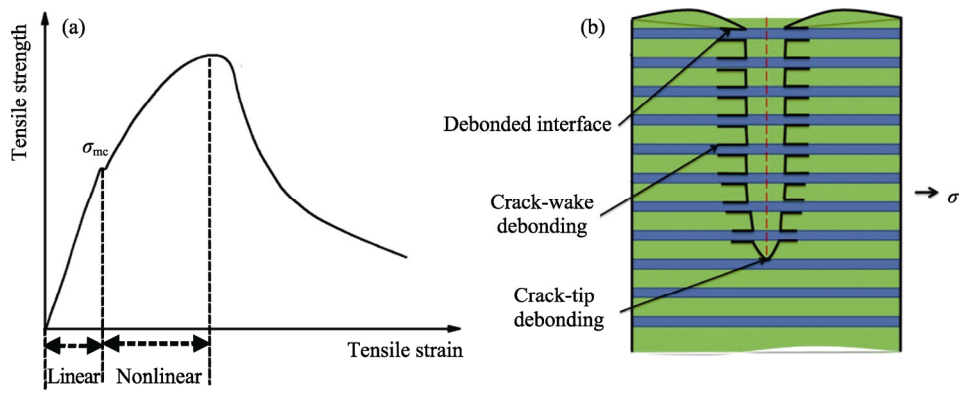

Fig. 1 (a) Typical tensile stress–strain curve of unidirectional ceramic matrix composites; (b) schematic representation of a short matrix crack in a unidirectional composite, in which the fibers remain intact. Reproduced with permission from Ref. [19], © Institute of Materials, Minerals and Mining and ASM International 2016.

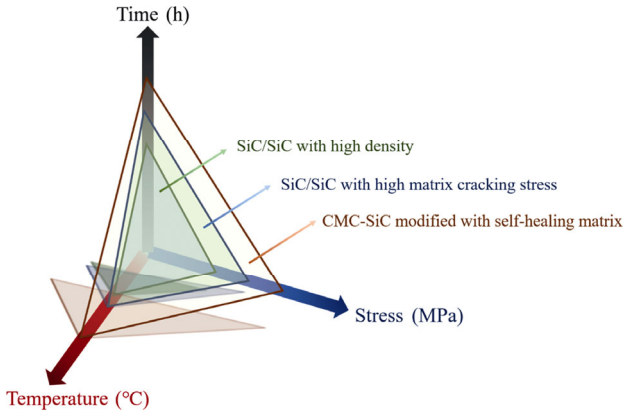

Fig. 2 Different types of CMC-SiC used for different service conditions (stress, temperature, and time).

under the influence of above two factors. The oxygen is blocked outside, and the duration is prolonged. The self-healing components, usually containing B element, BC_x [29–34], SiBC [35–41], and SiBCN [42], are the mainly self-healing components used to modify CMC-SiC [43]. The B_2O_3, B_2O_3–SiO_2 (borosilicate glass), and SiO_2 glass could be generated from the oxidation of the above self-healing components [44]. The good viscous flow and wettability of glass phase with SiC matrix promote the healing of matrix microcracks. The ZrO_2–SiO_2 [45–48] and HfO_2–SiO_2 [49] glass may be two kinds of promising self-healing phase used at higher temperatures in the future.

In this paper, the measures to obtain long-term CMC-SiC are proposed and discussed. High degree of densification, high σ_{mc}, and introduction of the self-healing components are three significant strategies to prolong the duration of CMC-SiC. The corresponding manufacture technologies to obtain CMC-SiC with high densities are elaborated. The design principles of fiber preform architecture, interface shear strength, CTE match, and matrix strengthening are summarized to enhance the σ_{mc}. The types of self-healing component and the effective self-healing temperature range are first distinguished and concluded. The self-healing mechanism is deeply discussed. The CMC-SiC with excellent service performance can be obtained by the microstructure and composition design combined with proper process technique. This review could help reader quickly familiarize the progress and major scientific issues of the long-term CMC. The principles of the process control, microstructure design, and composition choice are further provided for researchers to fabricate CMC with excellent characteristics (e.g., mechanical property and self-healing performance). The development tendency of the thermal-structure composites for aeroengine is predicted, and the valuable thinking space is built for subsequent researchers.

2 SiC/SiC with high densities

As for some components working at low stress, the stress damage could be neglected, and the oxidation damage is fatal for SiC/SiC. The interphase and fiber would be rapidly oxidized, resulting from the diffusion of oxygen through pores, which are derived from the preparation technology. The SiC/SiC would quickly fail, and the duration significantly declined. In this situation, improving the degree of densification is a kind of effective approach for enhancing the environment property. The dense oxidation layer generated on the surface of SiC/SiC with high densities can prevent the diffusion of oxygen. The oxygen is blocked outside the composites, and the service life is hopeful to be increased. In addition, the pores can act as crack origin and enhance the interface thermal resistance. The mechanical property and thermal conductivity of SiC/SiC could also be improved if the pores can be eliminated as far as possible. The methods for preparing CMC with high densities are summarized in Section 2.

2.1 Melt infiltration (MI) technology

MI is one kind of the methods to obtain SiC/SiC with high densities. Lots of investigations about SiC/SiC via MI have been done by National Aeronautics and Space Administration (NASA) [1,50–53]. The 5-harness satin fabrics (Sylramic-iBN SiC fibers) were stacked and squeezed in a graphite fixture. Then, the Si–B–N interphase coating and a layer of SiC matrix over-coating were produced outside SiC fiber by the CVI. The obtained semi-dense SiC/SiC contained open porosity ranging from 20 to 30 vol%. Next, the SiC particles were introduced into semi-dense SiC/SiC by the slurry infiltration (SI) process. The residual big space between fiber bundles was divided into small pores by SiC particles. Finally, the residual small pores were filled by molten silicon near 1400 ℃. Comparing with RMI, there is no chemical reaction during the MI process. The silicon can fill almost all of the open pores by the effect of capillary force. Thus, the density of SiC/SiC can reach a higher level.

The microstructures of the as-fabricated composites are shown in Fig. 3 [50]. The fiber volume fraction is

36%, and the contents of Si–B–N interphase, CVI SiC, SiC particles, and silicon are about 8, 23–35, 6–18, and 13–18 vol%, respectively. The open porosity is about 2%, and the density can reach 2.85 g/cm^3. Until now, various SiC/SiC systems (N-22, N24-A, N24-B, and N24-C) with working temperatures from ~1200 ℃ to over 1315 ℃ have been developed by NASA. As shown in Table 1, the tensile strength of SiC/SiC via MI can reach 400–450 MPa, and the value of σ_{mc} is in the range of 160–180 MPa at room temperature. The rupture life of N24-C is more than 1000 h when it is applied under the load of 103 MPa in air at 1315 ℃ [54–56].

The usage temperature of MI SiC/SiC is limited as a result of the existence of Si. The sweating of residual Si in rotating components is detrimental to surrounding metallic sub-components when they work above 1400 ℃. The degradation of SiC fiber and interphase is another reason causing the decrease of mechanical property beyond 1250 ℃. Bhatt *et al*. [57] researched the microstructure evolution after SiC/SiC was exposed to flowing air for 100 and 500 h at 1300–1400 ℃. The tensile property was also tested before and after each exposure condition. With the increase of exposure temperature, the modulus, σ_{mc}, and tensile strength declined. The residual Si diffused through the CVI SiC coating and attacked BN interphase and SiC fiber. After SiC/SiC was exposed at 1400 ℃ for 500 h, the ultimate tensile strength decreased to about 50% of that before exposure. Dicarlo *et al*. [58] further established a simple diffusion-based analytical model to predict the effect of stress-free thermal exposure on the residual tensile strength of MI SiC/SiC. It was meaningful to avoid the catastrophic damage if the duration can be properly predicted after MI SiC/SiC was fabricated.

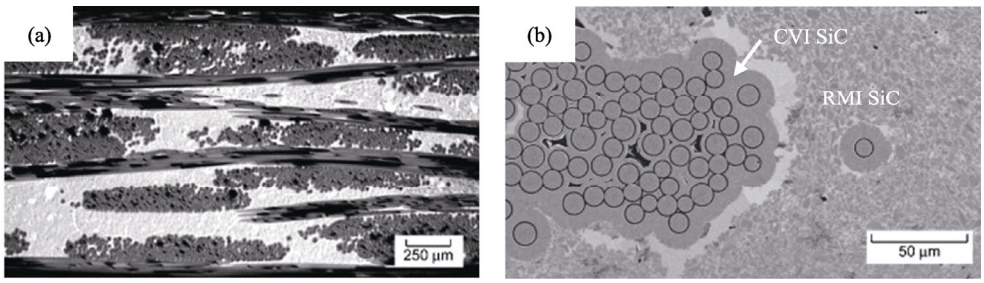

Fig. 3 Cross-section morphologies of the as-fabricated MI SiC/SiC with high degree of densification: (a) distribution of SiC fiber cloth and matrix phase; (b) microstructure details of the SiC fiber tow and SiC matrix. Reproduced with permission from Ref. [50], © Elsevier B.V. 2007.

Table 1 Average mechanical properties for NASA-developed CMC systems (2D 0/90 test panels with ~36 vol% total fiber content) [44]

Test temperature (℃)	Property[a]	CMC system			
		N22	N24-A	N24-B	N24-C
20	Upper use temperature (℃)	1204	1315	1315	1315
	Initial elastic modulus (GPa)	250	250	210	220
	Proportional limit stress (PLS) (MPa)	180	180	170	160
	Ultimate tensile strength (MPa)	400	450	450	310
	Ultimate tensile strain (%)	~0.35	~0.55	~0.50	~0.30
	Interfacial shear strength (MPa)	~70	~70	~7	< 7
800	Ultimate tensile strength retention after 100 h burner rig (%)	60	100	100	—
	Rupture strength (100 h, air) (MPa)	200	200	240	—
At or near upper use temperature	PLS (MPa)	170	170	160	150
	Ultimate tensile strength (MPa)	320	380	380	260
	Creep strain (103 MPa, 500 h, air) (%)	~0.4	~0.4	~0.4	0.2
	Creep strain (69 MPa, 500 h, air) (%)	—	0.15	0.15	0.12
	Rupture life (103 MPa, air) (h)	~500	~500	~500	> 1000

[a] Mechanical properties measured in-plane in the 0° direction with a directional fiber content of 18 vol%.

2. 2 Nano-infiltration and transient eutectic-phase technology

Nano-infiltration and transient eutectic-phase (NITE) process is another method to fabricate SiC/SiC with high densities. Kohyama *et al*. [59–61] had done a lot of work on this technology for nuclear fusion reactor. In their investigation, Tyranno-SA SiC fiber was employed as the reinforcement. The pyrocarbon (PyC) or $(PyC/SiC)_n$ multilayered interphase was prepared in SiC fiber preform by the CVI. The SiC matrix was formed via transient liquid-phase sintering of mixed powders containing nano β-SiC and a small amount of sintering additives, such as Al_2O_3 and Y_2O_3. Finally, the SiC/SiC can be obtained after hot-pressed sintering at the temperature range of 1720–1780 ℃ and the pressure range of 15–20 MPa. The density of SiC/SiC can reach 2.96 g/cm^3, and the open porosity decreased to 3.7%. The increase of density also makes great contribution to the rise of σ_{mc} [59]. Thermal exposure test of NITE SiC/SiC was carried out at 1000 ℃, and the recession of PyC interphase was not found [62]. It means that the oxygen is blocked outside of SiC/SiC, and the environment property is dramatically improved.

3 SiC/SiC with high matrix cracking stress

σ_{mc} is a significant parameter for CMC. If the working stress exceeds σ_{mc}, the matrix microcracks would rapidly come into being. The oxygen could diffuse into samples along the matrix microcracks. The service duration would dramatically decline, resulting from the oxidation of interphase and fiber. Increasing the σ_{mc} is an effective strategy to ensure that CMC can serve in non-damaged state to achieve long-term work target.

Sigl and Evans [63] studied the crack growth resistance and matrix cracking stress of CMC. The matrix cracking stress can be expressed by Eq. (1):

$$\frac{\sigma_0}{E}+\frac{\sigma_m^R}{E_m}=\left[\frac{6\mu f^2 E_f G_{mc}}{(1-f)E_m E a}\right]^{1/3}\left(\frac{q}{E_m}\right)^{1/3} \quad (1)$$

where σ_0 is the matrix cracking stress; σ_m^R is the axial residual stress in matrix; G_{mc} is the matrix toughness; E, E_m, and E_f are the Young's moduli of composites, matrix, and fiber, respectively; μ is the friction coefficient; f is the fiber volume fraction; a is the fiber radius; and q is the normal compressive stress at the interface. According to Eq. (1), σ_0 is proportional to f and q. It means that the matrix cracking stress is increased with the addition of fiber volume fraction and normal compressive stress at the interface. When the σ_m^R is negative, it means that there is residual compressive stress in matrix, and σ_0 increases. The CTE in the axial direction of matrix is required to be less than that of fiber to ensure the residual compressive stress in the matrix. The CTE in the radial direction of matrix is required to be more than that of fiber to obtain residual compressive stress at the interface. The interface shear strength is enhanced with increased q, and excellent stress transfer ability from matrix to fiber is ensured.

According to Morscher *et al*. [64–66], the matrix cracks originate in the 90° minicomposites for two-dimensional (2D) and three-dimensional (3D) architectures with 0°/90° characteristic, which consist of 90° fiber, interphase, and matrix. The matrix cracking is related to the stress in the matrix region of 90° minicomposites, which is termed as mini-matrix. This mini-matrix stress $\sigma_{mini\text{-}matrix}$ can be determined from simple rule-of-mixture theory:

$$\sigma_{mini\text{-}matrix}=\frac{(\sigma_T+\sigma_{th})}{E_c}\left(\frac{E_c-f_{mini}E_{mini}}{1-f_{mini}}\right) \quad (2)$$

where σ_T is the applied tensile stress; σ_{th} is the residual compressive stress in matrix; E_c is the composite elastic modulus; f_{mini} is the fiber volume fraction of 0° minicomposites (which consist of 0° fiber, interphase, and matrix) in the loading direction; and E_{mini} is the elastic modulus of 0° minicomposites, which can be calculated by the rule-of-mixture with the elastic modulus and volume fraction of each constituent in 0° minicomposites. It demonstrates that the matrix cracking stress is significantly dependent on the residual stress in the matrix, fiber volume fraction, and elastic modulus of 0° minicomposites. In a word, four factors including the fiber preform architecture (fiber volume fraction in the loading direction), interface shear strength, residual stress (CTE match), and elastic modulus of 0° minicomposites (matrix strengthening) affect σ_{mc} (Fig. 4).

3. 1 Fiber preform architecture

The fiber volume fraction is required to at least 20% in the CMC-SiC. Therefore, the fiber preform structure has significant effect on σ_{mc}. The matrix cracking behavior of SiC/SiC with different fiber architectures was compared by Morscher *et al*. [67]. The model of different preform architectures was built. Acoustic

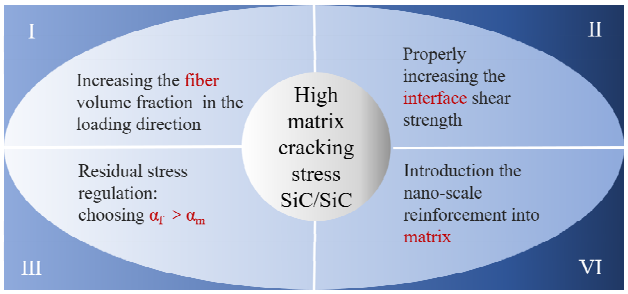

Fig. 4 Methods to increase the matrix cracking stress of SiC/SiC composite.

emission (AE) was employed to monitor the matrix cracking phenomenon. It indicated that the increased fiber volume fraction in the loading direction and lower transverse fiber tow perpendicular to the loading direction were beneficial to the increase of PLS, and the matrix cracking behavior was correspondingly delayed. According to the rule of mixture, the tensile strength of composite during the liner elastic deformation stage can be calculated according to Eq. (3):

$$\sigma_c = \sigma_f \upsilon_f + \sigma_m \upsilon_m \tag{3}$$

where σ_c, σ_f, and σ_m are the strengths of composite, fiber, and matrix, respectively; and υ_f and υ_m are the volume fractions of fiber and matrix, respectively. According to Eq. (3), σ_c improves with the increase of υ_f. If the number of 90° fiber was greater with the same total fiber volume fraction, the source of through-thickness matrix cracks would form in the 90° minicomposites at low stress. As for 2D-woven 0°/90° SiC/SiC loaded in the 0° direction, the σ_{mc} was also controlled by the size of 90° minicomposites. The width of the tunnel crack was wider when the size of 90° minicomposites is larger [66]. The value of σ_{mc} was higher when the tow size of the *Z*-direction fiber was smaller for 3D-woven composites [65].

The energy balance approach was employed by Li [68] to investigate the relationship between σ_{mc} of CMC and other parameters. The results showed that σ_{mc} increased with the increase of fiber volume fraction, fiber strength, interface debonded energy, and interface shear stress. In Ref. [69], the effect of interface debonding on matrix multi-cracking was further investigated. The Budiansky–Hutchinson–Evans shear-lag model was used to analyze the stress distributions in fiber and matrix. The fracture mechanics approach was adopted to calculate the interface debonding length. The unit cell of composites was built, and the theoretical prediction was done. The experimental results agreed well with the theoretical prediction. It indicated that the σ_{mc}, matrix cracking saturation stress, and saturation matrix crack density were enhanced by increasing the fiber volume fraction and interface shear stress.

3. 2 Interface shear strength

Though the volume fraction of interphase is low, it has significant effect on the property of CMC [70–72]. The interphase plays the role of mechanical fusing and load transfer, protecting the fiber from chemical damage and relieving residual stress [70,73,74]. Hence, the interface shear strength, who acts as the most important interphase characteristic, also has significant impact on σ_{mc}.

Zhu *et al*. [75] introduced bubble-chain boron nitride nanotubes (BNNTs) into SiC/SiC (Fig. 5) to play the role of interphase. The interfacial bonding strength was enhanced by the as-grown or BN-coated BNNTs compared with conventional BN interphase via the CVI. The damage initiation and evolution were monitored by the AE. The results showed that the PLS obtained from the stress–strain curve increased from 104.6 to 130.9 MPa after the BNNTs were introduced into interphase. The AE onset stress acquired from the AE energy–stress figure, and the number of high energy events was further enhanced when the BNNTs were introduced. It means that the damage initiation was postponed, and more energy was consumed when the cracks propagated. Increased service life could be predicted due to high σ_{mc}. The carbon nanotubes (CNTs) were introduced into the PyC interphase of SiC/SiC via electrophoretic deposition by Feng *et al*. [76]. The SiC/SiC with PyC interphase and CNTs–PyC interphase was signed as SiC/SiC–P and SiC/SiC–CP, respectively. The interface shear strength (τ_i) and flexural strength were compared. The τ_i was more than 55 MPa after adding the CNTs. It increased more than two times compared with SiC/SiC–P. The load–displacement curve of SiC/SiC–CP was steeper, and it indicated that the modulus and rigidity were significantly improved. The load can be quickly transferred from matrix to fiber when τ_i increases. The matrix cracking tendency can be delayed. As shown in Fig. 6, the tensile stress (σ_T) is applied to the sample. If the value of τ_i is higher, the stress can be transferred from matrix to fiber quickly. The stress in matrix (σ_m) can be calculated by the difference between σ_T and the stress in fiber (σ). The stress in the matrix of composites with higher

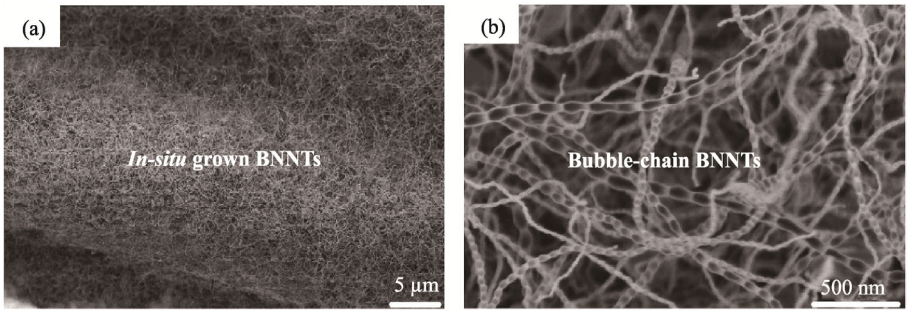

Fig. 5 (a) Typical scanning electron microscopy (SEM) images of the as-grown BNNTs on SiC fiber; (b) partial enlarged images of BNNTs. Reproduced with permission from Ref. [75], © Elsevier Ltd. 2018.

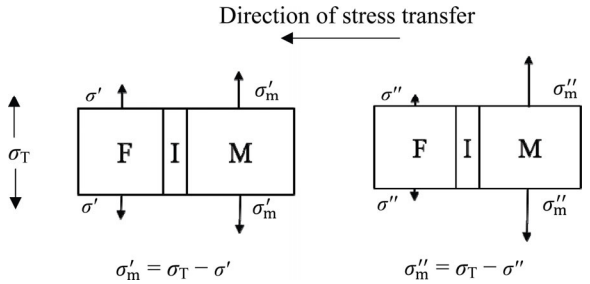

Fig. 6 Schematic diagram of stress transfer in composites. F, I, and M represent fiber, interphase, and matrix, respectively.

τ_i (σ'_m) can be marked as $\sigma'_m = \sigma_T - \sigma'$, where σ' is the stress in the fiber with higher τ_i; and the stress in the matrix of composites with lower τ_i (σ''_m) can be estimated by $\sigma''_m = \sigma_T - \sigma''$, where σ'' is the stress in the fiber with lower τ_i. σ'_m is lower than σ''_m because σ' is greater than σ''. The matrix crack initiation could be deferred up to higher applied stress, and the composites would serve without damage for a long time.

3. 3 CTE match

The CTE (α) match should be properly designed for long-lifetime SiC/SiC. The CTE of fiber (α_f) at axial direction should be higher than that of matrix (α_m) to obtain axial residual compressive stress in matrix. The applied tensile stress minus residual compressive stress is the actual tensile stress in matrix. The crack initiation is delayed up to higher applied stress. The α_f at radial direction should be lower than α_m. The radial residual compressive stress at interface area makes great contribution to the increase of interface shear strength, and the σ_{mc} is correspondingly improved.

The 2D SiC/SiC using two kinds of SiC fiber (Hi-Nicalon SiC fiber and Sylramic-iBN SiC fiber) was fabricated via the CVI by Morscher *et al*. [77]. The α of Hi-Nicalon SiC fiber, Sylramic-iBN SiC fiber, and CVI SiC matrix is about 3.5×10^{-6}, 5.4×10^{-6}, and 4.6×10^{-6} K^{-1} [78], respectively. The residual stress was determined by the load–unload–reload hysteresis test. The residual tensile stress existed in matrix of Hi-Nicalon SiC/SiC attributed to $\alpha_{f(Hi\text{-}Nicalon)} < \alpha_{m(CVI\ SiC)}$, and the value was only about 0–10 MPa. Owing to $\alpha_{f(Sylramic\text{-}iBN)} > \alpha_{m(CVI\ SiC)}$, the residual stress was the compressive stress in the matrix of Sylramic-iBN SiC/SiC, and the value was in the range of 25–42 MPa. The residual compressive stress can offset part of applied stress. The results showed that the σ_{mc} range of Hi-Nicalon SiC/SiC was approximately 80 MPa lower than that of Sylramic-iBN SiC/SiC with similar fiber volume fraction in the load direction. It indicated that the residual stress made great contribution to the stress-dependent σ_{mc}.

3. 4 Matrix strengthening

The one-dimensional (1D) nanomaterials (SiC nanowire, CNTs, BNNTs, etc.) with high strength and modulus are a kind of significant reinforcement similar to fiber. Many efforts have been made to introduce the 1D nanomaterials into matrix of CMC. The load can be quickly transferred to 1D nanomaterials from matrix when composites are loaded. The modulus of composite matrix is enhanced, and the matrix cracking is expected to be postponed up to higher stress.

Pavia *et al*. [79] extended the classical Aveston–Cooper–Kelly shear-lag model to hybrid brittle matrix composite, which contained both micro-scale and nano-scale fibers to predict the matrix cracking stress. The foundational composite (Nicalon SiC fiber reinforced SiC matrix via the CVI) was employed. The property parameter of nano-scale fiber referred to the property of CNTs. The effect of nanofiber volume fraction on the σ_{mc} is shown in Fig. 7. The addition of nanofiber had remarkable effect on the σ_{mc}. It indicated that the σ_{mc} increased with the enhancement of volume fraction

and modulus of nanofiber. In addition, increased interface friction sliding stress and decreased nanofiber radius made great contribution to the increase of the σ_{mc}. The σ_{mc} of nanofiber reinforced composites, which had the same reinforcement volume fraction as hybrid composites, was also obtained and compared with that of hybrid composites. It indicated that the presence of Nicalon microfiber was beneficial to further increase σ_{mc}. The "hybrid effect" existed in this kind of micro/nanohybrid composites. Park *et al*. [80,81] investigated the mechanical property of SiC/SiC fabricated by whisker growing assisted CVI process. The SiC whisker was successfully introduced into 2D plain wave SiC preform via *in-situ* growing. The flexural strength of SiC whisker-modified SiC/SiC with the density of 2.71 g/cm^3 was further enhanced to about 610 MPa. Kim *et al*. [82] studied the microstructure and mechanical property of the SiC nanowire-modified SiC/SiC. The SiC nanowires were grown into SiC fiber preform using CH_3Cl_3Si (MTS)–H_2 system via the CVI process. The grain size of CVI SiC matrix decreased after the introduction of SiC nanowires, resulting from the increase of deposition sites, and more impingements of the growth fronts came into being. The columnar SiC crystals grew radially on the surface of SiC fiber in SiC/SiC (Fig. 8(a)). However, the SiC matrix was uniformly deposited on the surface of SiC fiber and SiC nanowires. No obvious growth direction was observed in the SiC nanowire-modified SiC/SiC (Fig. 8(b)). The flexural strength, modulus, and rigidity obtained in flexural stress–displacement curve (Fig. 8(c)) were significantly enhanced with the addition of SiC nanowires, which was related to the matrix strengthening effect.

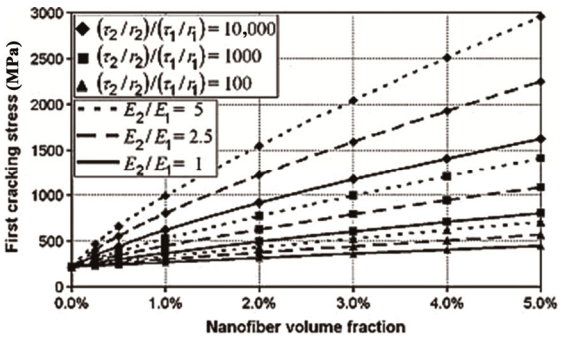

Fig. 7 Matrix cracking stress vs. nanofiber volume fraction of micro/nanohybrid composite with different nanofiber properties. E_1 and E_2 are the moduli of microfiber and nanofiber, respectively; τ_1 and τ_2 are the interface friction sliding stress; and r_1 and r_2 are the microfiber and nanofiber radii, respectively. Reproduced with permission from Ref. [79], © Elsevier Ltd. 2010.

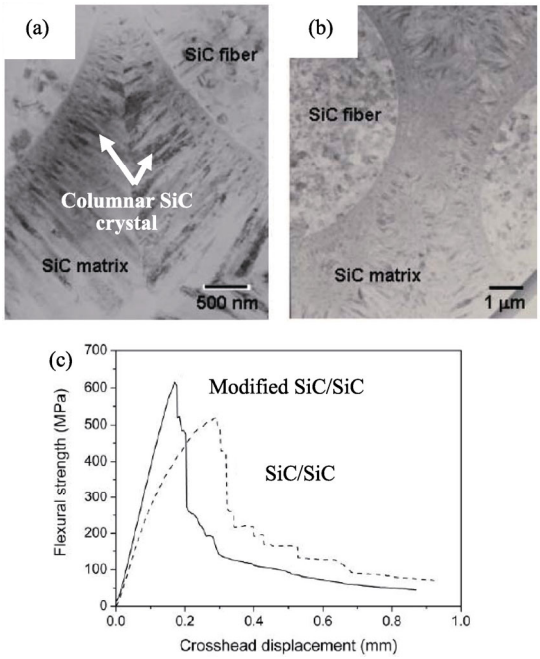

Fig. 8 Transmission electron microscopy (TEM) micrographs of (a) SiC/SiC, (b) SiC nanowire-modified SiC/SiC, and (c) the flexural strength vs. displacement curves of two kinds of composites. Reproduced with permission from Ref. [82], © Trans Tech Publications, Switzerland 2009.

4 CMC-SiC modified with self-healing matrix

When the applied stress is higher than σ_{mc}, the matrix microcracks acting as the oxygen diffusion pathway would initiate and propagate. The oxidation of interphase and fiber is the most fatal damage for SiC/SiC. On the one hand, the glass phase can be directly introduced to SiC/SiC. The cracks would be sealed by the viscous flow of glass phase at high temperatures. On the other hand, the self-healing component (B_xC, SiBC, SiBCN, B-containing compounds, etc.) is employed to prolong the duration. The B_2O_3 or borosilicate glass is generated from the oxidation of self-healing component at the crack surface. Meanwhile, volume expansion exists when the self-healing component oxidizes. The cracks would be quickly closed with the effect of the above two factors, and oxygen is blocked outside.

Self-healing is the response of material when it is loaded in high-temperature and oxidizing environment. The relationship between service conditions and self-healing performance of self-healing ceramic matrix composite (SHCMC) is shown in Fig. 9. The heat and oxidizing atmosphere significantly affect the oxidation rate of self-healing component (as well as the production

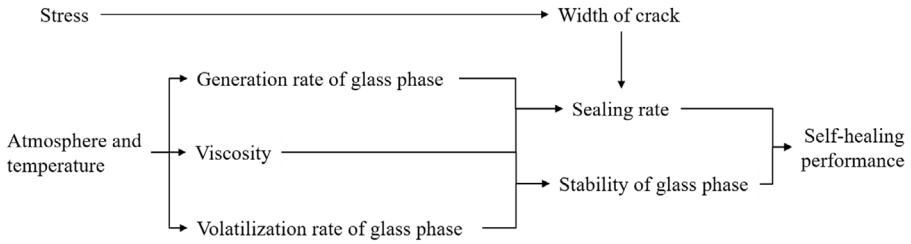

Fig. 9 Relationship diagram between service conditions and self-healing performance of SHCMC.

rate of glass phase), volatilization rate, and viscosity of glass phase. The production rate and viscosity of glass phase determine the healing rate. The glass phase stability is dependent on the volatilization rate and viscosity. In order to obtain excellent self-healing property, the healing rate should be as far as possible, and the glass phase stability should be excellent. With the increase of temperature, the oxidation rate of self-healing components is faster, and the glass phase formation rate is correspondingly quicker, which is good for crack healing. Simultaneously, the viscosity decreases, and the volatilization rate increases [83]. The cracks would be opened again, and the internal material would be exposed to oxygen again. If the temperature is too low, the oxidation rate of self-healing component is too slow to form a sufficient glass phase. Meanwhile, the viscosity of glass is too high to flow. The cracks are difficult to be quickly filled though the volatilization rate of glass is rather slow. It means that the self-healing phenomenon only occurs at particular temperature range. The value of stress controls the crack width. The higher the stress, the wider the crack is. Longer time is needed to generate enough self-healing phase and fill the cracks. The healing rate is slower, and self-healing performance is poor. Above all, the self-healing component should be properly chosen to ensure the high forming rate, low volatilization rate, and suitable viscosity of self-healing phase. The microstructure of SHCMC should be precisely designed to decline the crack width and crack density when it is loaded.

According to the above analysis, the stability of glass phase has significant impact on self-healing performance. Different glass phases have different melting points. It means that the viscosity and volatilization rate of different glass phases are different at the same temperature. The effective operating temperature ranges of various glass phases are correspondingly different, and they are summarized in Fig. 10. The melting point of B_2O_3 is about 450 ℃. Its effective protection effect works at 450–900 ℃ [30,32] because bubbles would come into being due to the high vapor pressure beyond 900 ℃ [84]. At 1000–1200 ℃, the borosilicate glass shows suitable viscosity and good wettability. The effective operating temperature range of borosilicate glass is 1000–1200 ℃ [85]. The SiO_2 glass shows excellent self-healing property when the temperature is above 1200 ℃. Because the melting point of SiO_2 is about 1723 ℃, the viscosity of SiO_2 is low, and the vapor pressure is high above 1400 ℃. The diffusion rate of oxygen through SiO_2 scale increases. The SiO_2 makes great contribution to the crack healing at the temperature range of 1200–1400 ℃. When the temperature is more than 1400 ℃, Al_2O_3 can be added to improve the stability of SiO_2 [86,87]. In addition, the refractory metal oxide, like ZrO_2 or HfO_2, also can be introduced to stabilize the SiO_2 in view of the formation of ZrO_2–SiO_2 or HfO_2–SiO_2 glass by the solution of refractory metal oxide in SiO_2. The melting point of refractory metal oxide correspondingly decreases [88] according to the ZrO_2–SiO_2 and HfO_2–SiO_2 phase diagrams [89–94]. In addition, Reactions (4) and (5) between SiO_2 and SiC are severe above 1700 ℃ [95,96]:

$$SiC(s) + SiO_2(s) + 1/2O_2(g) \rightarrow 2SiO(g) + CO(g) \quad (4)$$

$$SiC(s) + 2SiO_2(s) \rightarrow 3SiO(g) + CO(g) \quad (5)$$

The bubbles would appear in SiO_2 scale with the formation of SiO gas, and the oxide scale integrity would be damaged. The consumption of SiC matrix is also harmful to mechanical property. Reactions (4) and (5) may be also avoided with the enhancement of SiO_2 stability.

The self-healing components usually contain B element. The B-containing compounds can be rapidly oxidized, and sufficient B_2O_3 glass is produced. The B_2O_3 can further promote the oxidation of SiC according to Reaction (6) [44]:

$$7SiC(s) + 6B_2O_3(l) \rightarrow 7SiO_2(s) + 3B_4C(s) + 4CO(g) \quad (6)$$

The borosilicate glass can be generated with the solution

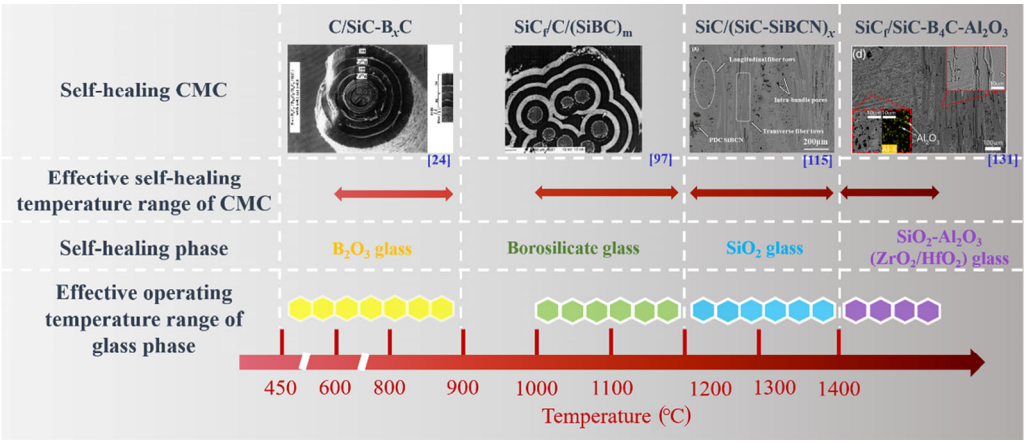

Fig. 10 Effective self-healing temperature range of different self-healing components and effective operating temperature range of different glass phases.

of SiO_2 in B_2O_3. The initial oxidation temperature and oxidation rate of various self-healing components are different at the same temperature. The effective operating temperature range of glass phase is also taken into account. The effective self-healing temperature range of different self-healing components is summarized in Fig. 10. For B_xC, the initial oxidation temperature is about 600 ℃ [97,98]. Though the effective operating temperature range of B_2O_3 glass is wide, the effective self-healing effect can be acquired until B_xC is oxidized. The effective self-healing temperature range of B_xC is about 600–900 ℃ (Fig. 10) [36,84]. The SiBC, which contains SiC crystallites and B_4C, begins to be oxidized at 800 ℃ [36]. The borosilicate glass is generated on the surface of SiBC at 800–1000 ℃. However, the viscosity of borosilicate glass is too high to flow at this temperature range, and the cracks are difficult to be closed. Sufficient and flowable borosilicate glass appears when the temperature is above 1000 ℃. Therefore, the effective self-healing temperature range of SiBC is about 1000–1200 ℃. The SiBCN begins to be oxidized at 900 ℃. The oxidation rate of SiBCN is low, and the glass phase is insufficient to seal the cracks below 1100 ℃ [99]. The SiBCN has great potential to heal the matrix microcracks at the temperature range of 1200–1400 ℃. The SiO_2 can be generated by the oxidation of SiC, and the initial temperature of SiC is about 800 ℃ [100]. However, the oxidation rate is low, and the viscosity of SiO_2 is too high at low temperatures. For SiC, the effective protection begins at about 1360 ℃ [41]. Above 1400 ℃, the volatilization of SiO_2 is severe. Furthermore, the active oxidation tendency of SiC increases when the temperature increases to 1500 ℃. The generated SiO gas is harmful to crack healing [49]. The effective self-healing temperature range of SiC is about 1360–1400 ℃. Above 1400 ℃, improving the stability of SiO_2 glass is the most significant issue. SiBCNAl, SiBCNHf, and SiBCNZr are considered to be suitable self-healing components. The oxidation products contain B_2O_3, SiO_2, Al_2O_3, ZrO_2, or HfO_2. The volatilization of SiO_2 can be inhibited owing to the solution of ZrO_2 or HfO_2 in SiO_2. The self-healing ability is expected to be provided by SiO_2–ZrO_2 [93] or SiO_2–HfO_2 glass [94] beyond 1400 ℃.

According to the effective operating temperature range of glass and effective self-healing temperature range of self-healing component, the composition of self-healing component can be properly designed for a certain temperature range. In addition, excellent self-healing performance can be obtained at a wide temperature range (800–1500 ℃) through the combination design of different self-healing components [101].

4.1 CMC-SiC modified with borosilicate glass

The self-healing behavior is quite complex. It includes the oxidation of self-healing components, crack sealing, and volatilization of glass phase. The self-healing phase, SiO_2–B_2O_3 glass, can be directly introduced into CMC-SiC to separately investigate the phenomenon of sealing cracks and glass stability. It is beneficial to analyzing the self-healing behavior of self-healing components.

Borosilicate glass coating was employed to prolong the worktime of C/SiC composite by Cheng *et al*. [102]. The sol–gel method combined with the sintering process (1000 ℃ for 1 h in vacuum) was conducted to fabricate SiO_2/B_2O_3 coating for C/SiC. The oxidation experiments were carried out at 400–1500 ℃ in air for

5 h, and the curves of weight loss and bending strength as function of oxidation temperature were recorded. Owing to the CTE mismatch between carbon fiber and SiC matrix, microcracks appeared in SiC matrix during cooling process from preparation temperature to room temperature. The microcracks are still open when the temperature is below the preparation temperature. The oxygen would quickly diffuse into C/SiC and oxidize the interphase and fiber. The results show that the weight loss rate of borosilicate glass-modified C/SiC was lower than that of the unmodified C/SiC from 400 to 1200 ℃ resulting from the self-healing effect of borosilicate glass (Fig. 11(a)). The oxygen was blocked outside, and thus the oxidation of PyC interphase and C fiber was prevented. The bending strength of the modified C/SiC was correspondingly higher than that of the unmodified C/SiC from 400 to 1200 ℃ (Fig. 11(b)). When the temperature was above 1200 ℃, the matrix microcracks were closed, and the evaporation of borosilicate glass was severe. The weight loss ratio and bending strength of the modified C/SiC and unmodified C/SiC were similar after oxidation. The borosilicate glass was also prepared on C/SiC brake material as self-healing coating [103]. The tetraethoxysilane ($Si(OC_2H_5)_4$, TEOS) and triethylborate ($B(OCH_3)_3$, TEOB) were used as the precursor for borosilicate glass. The oxidation test was conducted at 800 ℃ in air for 10 h. The weight loss of uncoated samples was about 40 wt%, and the carbon fiber was severely oxidized. However, with the protection of the borosilicate glass, the weight loss of coated samples was only 0.3 wt%. Excellent environment property of C/SiC composites was obtained with the addition of borosilicate glass.

The C/C composite is a significant material in aeronautics and astronautics field. However, the carbon would be oxidized above 450 ℃, and the wide application is limited. The SiC coating with excellent oxidation resistance is employed to protect C/C composite. However, microcracks with the average width of 2–3 μm exist in SiC coating owing to the CTE mismatch between SiC coating and C/C, which is harmful to oxidation resistance. Hatta *et al*. [44] added SiO_2–B_2O_3 glass coating with the thickness of about 100 μm outside SiC coating via the sol–gel method by a mixture of TEOS and TEOB. The microcracks in SiC coating were filled by the SiO_2–B_2O_3 glass. The oxidation tests were performed under a dry air flow of 200 mL/min at constant temperatures between 600 and 1600 ℃ for 1000 min. The melting points and evaporation temperatures of glass coatings, at which the bubbles came into being, were determined by direct observation using an optical microscope as a function of the ratio of SiO_2 to B_2O_3. The results showed that the maximum temperature for effective healing was improved about 200 ℃ with the addition of SiO_2 in borosilicate glass, and the evaporation rate was decreased. The borosilicate glass was also used as self-healing coating for SiC pre-coated C/C composites by Isola *et al*. [104]. The starting materials were 70.4 wt% SiO_2, 2.1 wt% Al_2O_3, 17.5 wt% B_2O_3, and 10 wt% BaO. The glass powders and ethanol were applied to SiC pre-coated C/C composites, and the samples were heated in a tubular oven at 1300 ℃ for 0.5 h. The borosilicate glass coating was marked as SABB glass. After oxidation at 1100 ℃ for 55 h, the mass loss of SABB glass-coated samples did not exceed 0.6%. Inversely, the mass loss of SiC coated C/C composites was over 60% after thermal cycling 20 h at 1100 ℃. It means that the oxidation of carbon phase was effectively hindered because the oxygen was blocked outside by borosilicate glass coating. Huang *et al*. [105] studied the oxidation property of borosilicate glass-modified SiC pre-coated carbon/carbon composites (SiC–C/C) in air at 1550 ℃ for 156 h. The borosilicate glass was

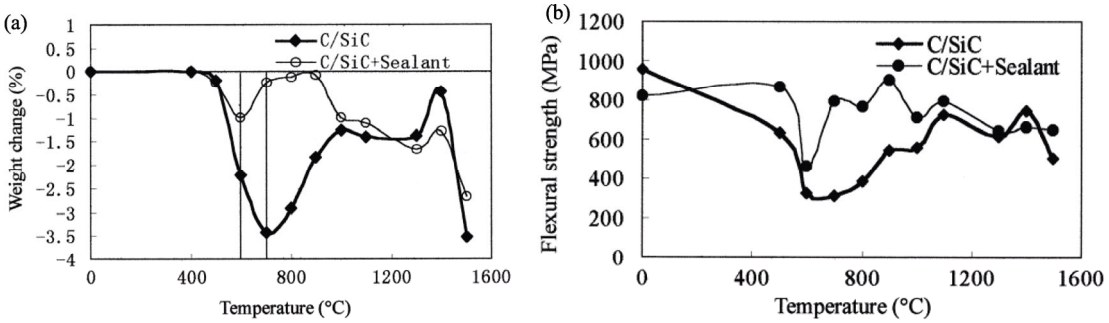

Fig. 11 (a) Weight change and (b) flexural strength after oxidation at different temperatures for 5 h. Reproduced with permission from Ref. [102], © Published by Elsevier Science Ltd. 2001.

fabricated by the pulse arc discharge deposition (PADD). After oxidation in air for 24 h at 1550 ℃, the mass loss of SiC–C/C composites was about 2.54%. However, the mass loss of the modified sample was only 1.20% after oxidation at 1550 ℃ for 156 h. In the stage of 0–12 h, the surface of borosilicate coating was rough, and some microholes appeared. The microholes can be attributed to the volatilization of B_2O_3 in borosilicate glass and some reactions occurred between SiC layer and glass layer according to Reactions (5), (7), and (8). With the increase of oxidation time, the microholes were healed by borosilicate glass. When the oxidation time was above 84 h, the volatilization of borosilicate was severe. Many holes and microcracks can be observed in the coating, and the self-healing performance was weak.

$$2SiC(s) + SiO_2(s) \rightarrow 2CO(g) + 3Si(s) \quad (7)$$

$$SiC(s) + SiO_2(s) \rightarrow C(s) + 2SiO(g) \quad (8)$$

The results show that the microcracks derived from the CTE mismatch between the fiber and matrix can be healed by the viscous flow of SiO_2–B_2O_3 glass. The interphase and fiber can be protected from oxidation, and the mechanical property of modified composites can be maintained. In addition, the melting point of SiO_2–B_2O_3 glass can be adjusted with a different SiO_2/B_2O_3 ratio. The self-healing temperature is correspondingly designable for specific service temperature. It provides a standard for the selection of self-healing components. The self-healing component with lower B content should be chosen to obtain SiO_2–B_2O_3 glass with higher melting points for higher service temperatures.

4. 2 CMC-SiC modified with self-healing component

When the self-healing components are introduced into the composites, the multilayered microstructure of matrix is usually designed, as shown in Fig. 12 [32]. The multilayered matrix consists of ceramic layers (SiC layer and B-containing compound layer) and alternative thin layer. The SiC matrix plays the role of carrying and transmitting the load. The thin layer is usually boron-doped pyrolytic carbon or BN, which can act as "mechanical fuse" phase to trigger crack deflection when cracks propagate in multilayered matrix. With the occurrence of crack deflection, the crack propagation pathway is prolonged. The energy is consumed, and the stress at crack tip is relieved. The sensitivity of multilayered matrix to crack opening is lower compared with a monolayered matrix. Meanwhile, the oxygen diffusion pathway is prolonged due to the crack deflection in the multilayered matrix. B-containing compound acts as the self-healing component, and the oxidation product can act as the sealant. Sufficient glass phase is formed at the crack surface and block the oxygen outside of the material. The interphase and fiber are protected from oxidation. The self-healing efficiency of multilayered matrix is improved on account of the effective debonding, crack deflection, and small crack width. Lots of investigations have been done on SHCMC with multilayered matrix.

4.2.1 CMC-SiC modified with BC_x

The SiC–BC_x multilayered matrix-modified C/SiC composites via the CVI were fabricated by Liu *et al*. [97]. The pores among filaments were filled by SiC matrix. The BC_x was located among SiC fiber bundles with alternative SiC matrix. The mechanical properties of modified composites at room temperature were similar with those of C/SiC. The residual strength of modified composites was similar to that of as-fabricated composites after oxidation at 700 ℃ for 10 h, and slight increase can be even observed after oxidation at 1000 and 1300 ℃ for 10 h in static air. The microcracks and

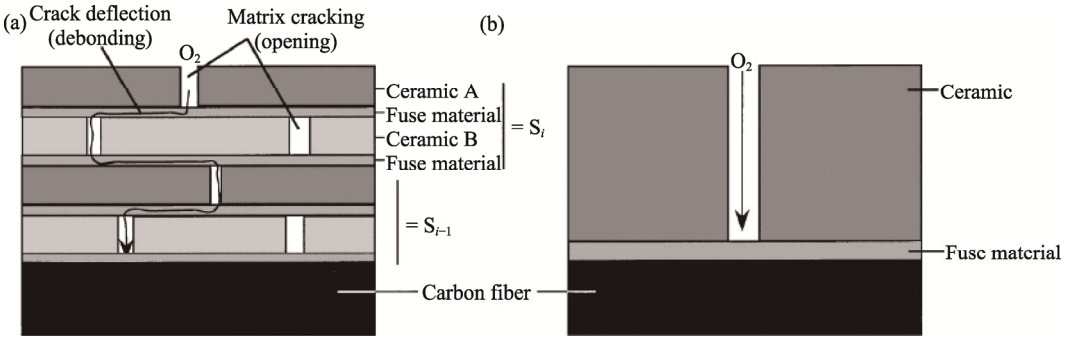

Fig. 12 Schematic representation of the compositions, damage propagations, and oxygen diffusion paths in (a) multilayered CMC and (b) monolayered CMC. Reproduced with permission from Ref. [32], © Elsevier Science Ltd. 1999.

pores on the surface were sealed by glass phase originating from the oxidation of multilayered matrix at 1000 and 1300 ℃. The interphase and fiber were protected from oxidation. The tensile strength retention ratios of modified composites were 95.44%, 93.55%, and 83.25% after exposed in the combustion environment (12% O_2/8% H_2O/80% Ar, 100 MPa, 700 ℃) for 10, 25, and 60 h, respectively. As shown in Figs. 13(b) and 13(d), the matrix cracks were healed by glass phase derived from the oxidation of multilayered matrix. As a comparison, the unmodified C/SiC fractured when it was tested in the combustion environment for 6.7 h. The creep tests in a wet oxygen atmosphere at 700 ℃ were also conducted [106]. The damage rate of C/SiC–BC_x composites was only about 0.95 MPa/h. The damage rate of C/SiC composites even reached 27.7 MPa/h. The damage rate correspondingly reduced 96.57% with the introduction of SiC–BC_x multilayered matrix, which indicated that the duration can be significantly prolonged compared with that of C/SiC composites.

The concept of multilayered and functional ceramic matrix was also been developed by Lamouroux *et al*. [32,33]. The unit sequence of functional matrix was B_xC_{1-x}/B_4C/B_xC_{1-x}/SiC. The B_xC_{1-x} with x = 0.1 played the role of mechanical fusion, and B_4C acted as the self-healing component. The lifetime of monolayered SiC matrix minicomposites and multilayered matrix minicomposites was measured with the tensile stress of 250 MPa at 700 ℃ in air. The lifetime of monolayered SiC matrix minicomposites was only a few hours. Whereas, the lifetime of multilayered matrix minicomposites was at least 100 h, and no rupture occurred after such long exposing time. The 2.5D C/SiC and multilayered C/SiC–B_xC composites were also fabricated. The morphology of rupture is shown in Fig. 14(a), and the successive layers of the matrix were observed. It proved the existence of crack deflection in multilayered ceramic matrix. The effective protection to interphase and fiber can be provided by this kind of multilayered ceramic matrix. The lifetime test was performed via four-point bending at 600 ℃ in air. The stress level corresponded to that of at tensile stress face. As shown in Fig. 14(b), the multilayered composites were loaded with the value of 100 MPa more than 180 h without fracture. Then, this sample was unloaded and reloaded at 180 MPa, and the rupture did not occur after 28 h in spite of the presence of above 0.6% strain on the tensile loaded face. The multilayered samples were loaded at 150 MPa, and they did not fail after 191 h. In contrast, the monolayered composites ruptured after exposure at 150 MPa for 10–30 h. The results show that the defects originated from preparation process or cracks initiated when CMC is loaded can be quickly healed at 600 and 700 ℃. Significant improvement of lifetime can be achieved by the design of multilayered SiC–B_xC matrix.

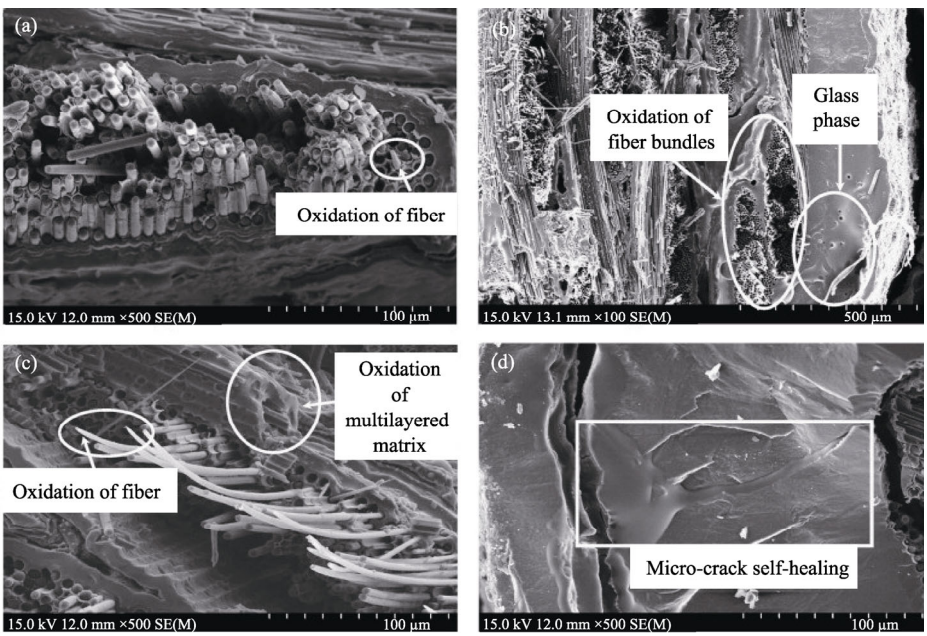

Fig. 13 Cross-section morphologies of the C/$(SiC–B_xC)_m$ multilayered composite after tensile tests at 700 ℃ and simulation combustion environment for different time: (a) 10 h, (b) 25 h, and (c, d) 60 h. Reproduced with permission from Ref. [97], © Published by Elsevier B.V. 2008.

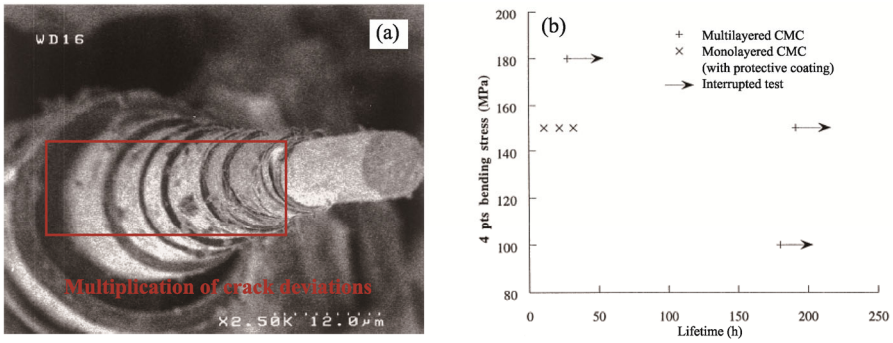

Fig. 14 (a) Rupture morphology of the multilayered C/SiC–B_xC composites after tensile test at room temperature; (b) lifetime of composites in four-point bending at 600 ℃ in an air atmosphere. Reproduced with permission from Ref. [32], © Elsevier Science Ltd. 1999.

4.2.2 CMC-SiC modified with SiBC

When the temperature is above 900 ℃, the self-healing effect of B_2O_3 glass is attenuated. Another self-healing component, which can product sealant with higher melting point, is needed. SiBC seems like a kind of suitable material for above problem, because borosilicate glass is generated when it is oxidized. Excellent self-healing effect could be obtained with the appearance of borosilicate glass at 1000–1200 ℃. There are two kinds of methods to obtain SiBC. One is the CVI process, and multilayered SiBC–SiC matrix can be acquired via alternative deposition of SiBC and SiC. The other is the RMI process. The microstructure and self-healing effect of two kinds of SiBC are discussed separately.

SiBC was fabricated by the CVI technique using MTS–BCl_3–H_2 system by Ye *et al*. [107]. The microstructure of SiBC was investigated by the TEM (Fig. 15). There were two kinds of crystals in SiBC ceramic, and they were evenly distributed. According to the energy dispersive spectroscopy (EDS) results, the two kinds of crystals were B_4C and SiC. And B_4C was surrounded by SiC. The oxidation behavior of SiBC was studied by Zhang *et al*. [38]. The SiBC coating was deposited on C/SiC composites. The oxidation test was conducted at 700, 1000, 1200, 1300, and 1400 ℃ for 6 h in a wet oxygen environment. The glass phase cannot be observed on the surface of the samples after oxidation at 700 ℃. However, according to the cross-section linear scanning of the EDS, the content of O element increased at the area closed to the surface. The Si–O bond can also be detected by the X-ray photoelectron spectroscopy (XPS). It meant that the SiBC began to be oxidized at 700 ℃. When the temperature increased to 1000 and 1200 ℃, glass phase can be seen at the surface of the samples. According to the XPS results, the borosilicate glass was generated with the oxidation of SiBC coating. The surface damage can be sealed and

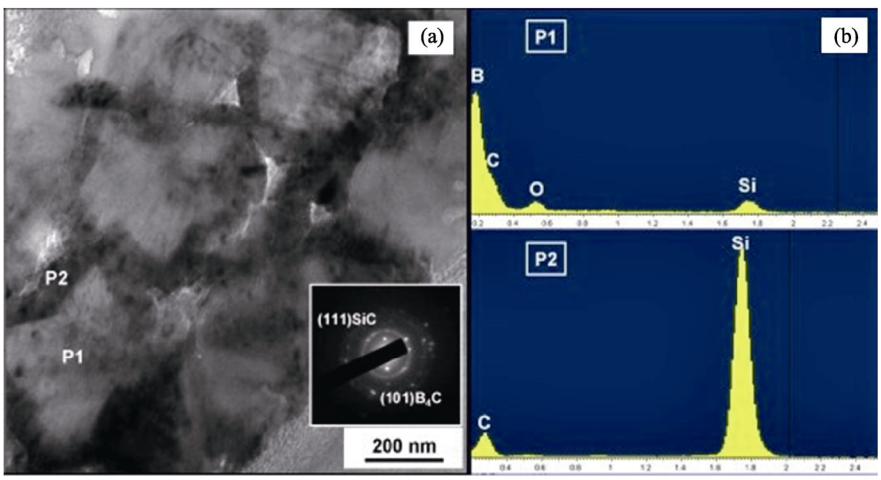

Fig. 15 (a) TEM image and (b) EDS analysis of CVI SiBC ceramic. Reproduced with permission from Ref. [107], © Published by Elsevier Ltd. 2012.

covered by the glass phase. Effective protection can be provided at the temperature range of 1000–1200 ℃. When the temperature was above 1200 ℃, the volatilization of borosilicate glass was severe. Many pores appeared in the oxidation scale, and the protection effect decreased. The results show that excellent self-healing property may be obtained when CMC is modified by SiBC at 1000–1200 ℃.

The SiBC was employed as the coating of C/SiC by Zuo *et al*. [98]. Three kinds of coatings were fabricated by the chemical vapor deposition (CVD), and they were SiC/SiBC/SiBC (labelled as A), SiC/SiBC/SiC (labelled as B), and SiC/SiC/SiC (labelled as C). The oxidation test was conducted at 700, 1000, 1200, and 1300 ℃ for 50 h in static air. The weight loss of Specimen A was more and more severe with the increased temperature. The carbon fiber was gradually oxidized because the volatilization rate of borosilicate glass was getting faster and faster when the temperature increased from 700 to 1300 ℃. Specimen B exhibited excellent weight stability at 1000–1300 ℃ due to good sealing ability and stability of borosilicate glass. The volatilization of glass phase can be prevented by the external SiC coating according to the self-healing mechanism (Fig. 16). However, the carbon fiber was oxidized because there was no sufficient glass phase after oxidation at 700 ℃, and the huge weight loss can be seen. The oxidation resistance of Specimen C with SiC coating was poor resulting from the low oxidation rate of SiC. The flexural strength before and after oxidation of C/SiC with different coatings was also measured. With the oxidation of fiber, the flexural strength of Specimen A decreased with the increase of oxidation temperature. Specimen B showed better flexural strength retention ratio at 1200 ℃ compared with Specimen A because the volatilization of glass phase was prevented by SiC coating. Specimen C exhibited the worst flexural strength retention ratio after oxidation at different temperatures on account of the lack of self-healing phase. The oxidation resistance of C/SiC with SiC/SiBC/SiC coating (SBS–C/SiC) was further investigated at a wet oxygen atmosphere for 50 h by Liu *et al*. [108]. The specimens were conducted in a wet oxygen atmosphere at 700, 1000, 1200, 1300, and 1400 ℃. The gas contents in the oxidizing atmosphere are 14 vol% H_2O/8 vol% O_2/78 vol% Ar (named as $14H_2O$ atmosphere) and 21 vol% H_2O/8 vol% O_2/78 vol% Ar (named as $21H_2O$ atmosphere). Reactions (9)–(19) might occur during oxidation test:

$$C(s) + O_2(g) \rightarrow CO_2(g) \quad (9)$$

$$B_4C(s) + 4O_2(g) \xrightarrow{600\,℃} 2B_2O_3(g) + CO_2(g) \quad (10)$$

$$B_4C(s) + 8H_2O \rightarrow 2B_2O_3(l) + CO_2(g) + 8H_2(g) \quad (11)$$

$$B_2O_3(l) \xrightarrow{600–1000\,℃} B_2O_3(g) \quad (12)$$

$$B_2O_3(l) + H_2O(g) \rightarrow 2HBO_2(g) \quad (13)$$

$$B_2O_3(l) + 3H_2O(g) \rightarrow 2H_3BO_3(g) \quad (14)$$

$$2SiC(s) + 3O_2(g) \rightarrow 2SiO_2(l) + 2CO(g) \quad (15)$$

$$SiC(s) + 3H_2O(g) \xrightarrow{\geqslant 1000\,℃} SiO_2(s) + CO(g) + 3H_2(g) \quad (16)$$

$$SiO_2(s) + 2H_2O(g) \rightarrow Si(OH)_4(g) \quad (17)$$

$$B_2O_3(l) + nSiO_2(l) \xrightarrow{1000\,℃} B_2O_3 \cdot nSiO_2(g) \quad (18)$$

$$B_2O_3 \cdot nSiO_2(g) \xrightarrow{\geqslant 1000\,℃} B_2O_3(g) + nSiO_2(s) \quad (19)$$

At 700 ℃, Reactions (9)–(14) occurred, and the cracks originating from the mismatch of CTE were partially healed by B_2O_3. The bending strength can be maintained to a certain extent. When the oxidation

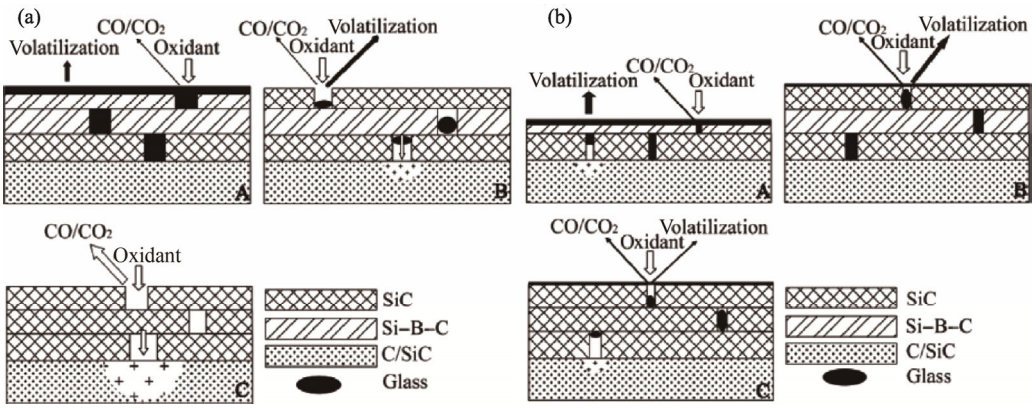

Fig. 16 Oxidation model of C/SiC with different kinds of coatings in static air: (a) below 1000 ℃; (b) above 1000 ℃. Reproduced with permission from Ref. [98], © Elsevier Ltd. 2012.

temperature increased to 1000 ℃, all above reactions would occur. The B_2O_3, SiO_2, and borosilicate glass appeared, and the cracks were well sealed. The flexural strength retention ratio even reached 106.7%. Above 1200 ℃, the volatilization rate of glass phase increased, and the protection effect decreased. Increasing the water partial pressure, the volatilization of glass phase was more severe because of Reactions (13), (14), and (17). The cracks were hard to be healed, and the strength decreased. The C_f/(SiC–SiBC)$_m$ with three layers of SiC coating (C/(SiC–SiBC)$_m$) and SBS–C/SiC were produced by Dong *et al*. [109]. As a comparison, the C/SiC with three layers of SiC coating (C/SiC) was also fabricated. The fatigue test was conducted in static air at 300, 550, 750, 1000, and 1200 ℃. The tensile stress and loading frequency of the fatigue test were 60±20 MPa and 0.5 Hz, respectively. At 300 ℃, the oxidation of carbon fiber has not started. The damage was formed under the effect of stress. The lifetime of all the three kinds of composites was more than 100 h. At 550 ℃, the glass phase originating from the oxidation of SiBC cannot be generated. The cracks were open, and the oxygen quickly diffused into composites. The carbon fiber was severely oxidized according to the fracture morphology after fatigue test. The lifetime of three kinds of composites dramatically decreased compared with that at 300 ℃. When the fatigue test was conducted at 750 ℃, the oxidation rate of carbon was faster. The oxidation of SiBC was slow, and only a small amount of cracks can be partially filled. The lifetime was mainly controlled by the oxidation of carbon fiber. The carbon fiber was also seriously oxidized in Fig. 17(a). The lifetime of samples modified with Si–B–C coating had a large dispersion, ranging from 7.5 to 47 h. The lifetime of C/(SiC–SiBC)$_m$ modified with SiBC matrix was 6.6 h. In contrast, the lifetime of C/SiC was only 1.5 h because the crack was always open. When the temperature increased to 1000 and 1200 ℃, the oxidation rate of SiBC was high enough to produce sufficient glass phase. The oxidation of carbon fiber was prevented in the polished cross-section morphology after fatigue test at 1000 ℃ (Fig. 17(b)). The lifetime at 1000 and 1200 ℃ was correspondingly increased compared with that at 750 ℃. The average lifetime of SBS–C/SiC modified with Si–B–C coating and C/(SiC–SiBC)$_m$ modified with SiBC matrix was 17 and 13 h, respectively. The average lifetime of two kinds of SiBC-modified C/SiC composites was longer than that of C/SiC.

Many scholars from other institutions have also studied the self-healing behavior of SiBC via the CVI. The fatigue behavior of SiC_f/(SiC–SiBC)$_m$ composites at 700 and 1200 ℃ was investigated [110]. The increase in modulus was observed after cyclic fatigue with the production of borosilicate glass. The oxidation of PyC interphase was inhibited because the cracks were sealed by glass phase, and the degradation of fiber/matrix bonding was correspondingly prevented. The fatigue lifetime of SiC_f/(SiC–SiBC)$_m$ composites at 100 MPa reached dozens of hours. When the fatigue stress increased to 120 MPa, the crack width was wider. The healing rate was correspondingly slower, and the lifetime decreased. In contrast, a premature failure existed in SiC/SiC. It ruptured after 1 h at 700 ℃ under a static stress of 100 MPa. Forio and Lamon [111] also researched the fatigue behavior of SiC_f/(SiC–SiBC)$_m$ composites. The results showed that the lifetime at 1100 ℃ was prolonged compared with that at 600 ℃ because of the formation of borosilicate glass by the oxidation of SiBC matrix in air. The cracks were quickly healed, and the PyC interphase was protected from oxidation. The pre-cracks had no

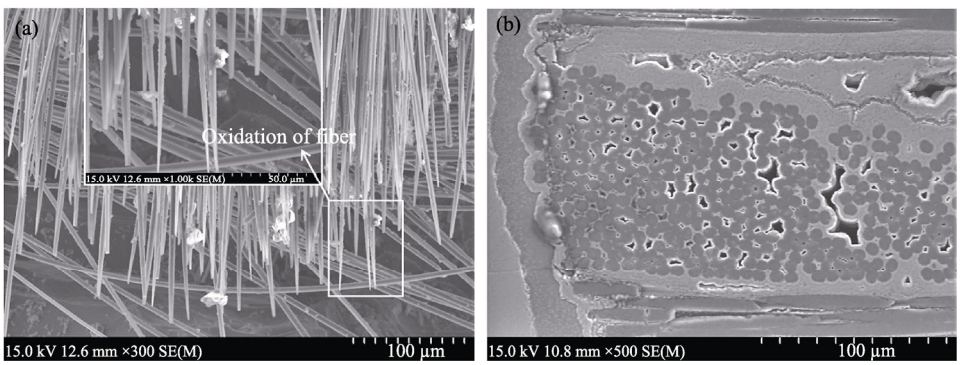

Fig. 17 (a) Fracture morphology after fatigue test of C/(SiC–SiBC)$_m$ at 750 ℃; (b) polished cross-section morphology after fatigue test of C/(SiC–SiBC)$_m$ at 1000 ℃. Reproduced with permission from Ref. [109], © Elsevier Ltd. 2016.

severe harm to lifetime. While, the applied maximum stress had significant effect on lifetime. The higher maximum stress made the wider crack, and the lifetime was shortened with decreased self-healing rate. The lifetime at different conditions is shown in Table 2. The oxidation behavior of multilayered $SiC_f/C/(SiBC)_m$ composites was investigated [112]. The $(SiBC)_m$ matrix consisted of three phases: SiC (Matrix 3), B_4C (Matrix 2), and SiBC (Matrix 1), and the microstructure is shown in Fig. 18(a). B_4C was closer to fiber, and the distance between SiBC and fiber was farther. SiBC was composed of SiC crystallites surrounded by an amorphous phase. The boron element existed as an amorphous boroncarbide phase or in SiC lattice. At 600 ℃, the PyC interphase was severely consumed because the oxidation rate of B_4C was too slow to form B_2O_3. The weight change curves were continuous and quasi-linear, as shown in Fig. 18(b). At higher temperatures (650 and 700 ℃), partial cracks were healed by B_2O_3 glass, and the oxidation of PyC was not as severe as that at 600 ℃. The weight loss was smaller with the intensified oxidation reaction of B_4C. At 800 ℃, the maximum weight gain was obtained. The oxidation rate of B_4C increased, and sufficient B_2O_3 glass was produced. The cracks were sealed, and the oxidation of PyC was prevented. At 900 and 1000 ℃, the viscosity of B_2O_3 glass decreased, and the partial B_2O_3 glass volatilized. The protection effect decreased, and PyC was oxidized. The weight gain decreased compared with that at 800 ℃. The weak oxidation of SiBC matrix can be observed at 1000 ℃, and the produced borosilicate glass made a small contribution to the weight gain and pore closure. When the oxidation temperature increased to 1200 ℃, the weight loss of nearly −0.07% was obtained at the first 50 min because of the volatilization of B_2O_3. Then, the weight gain (about 0.2%) from 50 min to 7 h was observed with the formation of borosilicate glass. The oxidation behavior was summarized in Table 3. The protection was mainly provided by B_2O_3 glass at 800 ℃. At higher temperatures of 1000–1200 ℃, the interphase was mainly protected from the oxidation by borosilicate glass. The $SiC_f/C/(SiBC)_m$ composites exhibit excellent self-healing ability at wide temperature range. The self-healing multilayered matrix (CVI-$(SiBC)_n$) composites have also been widely investigated by SNECMA, France, and several kinds of composites (A400, A410, and A500) were developed [113–116]. The lifetime via tensile fatigue and creep test performed at 120 MPa in air is shown in Fig. 19. The lifetime of A373 (SiC/SiC) rapidly decreased from dozen to several hours when the temperature increased from room temperature to about 850 ℃. The lifetime of A400 (with Nicalon fiber as the reinforcement) and A500 (with T-300 fiber as the reinforcement) was above 100 h until 1200 ℃. As for A410 (with Hi-Nicalon fiber as the reinforcement), the lifetime can reach 1000 h at 850 ℃ and 500 h at

Table 2 Lifetime of $SiC_f/(SiC–SiBC)_m$ composites in fatigue tests [111]

Specimen	Temperature (℃)	σ_{max} (MPa)	Precracking	Frequency (Hz)	Lifetime
1	600	150	No	0	12 h 3 min
2	600	150	No	0.25	15 h 20 min
3	600	150	Yes	0.25	13 h 23 min
4	600	250	No	0.25	4 h 2 min
5	1100	150	No	0	4 h 55 min
6	1100	150	No	0.25	52 h 32 min
7	1100	150	Yes	0.25	49 h 14 min
8	1100	220	No	0.25	2 h 10 min

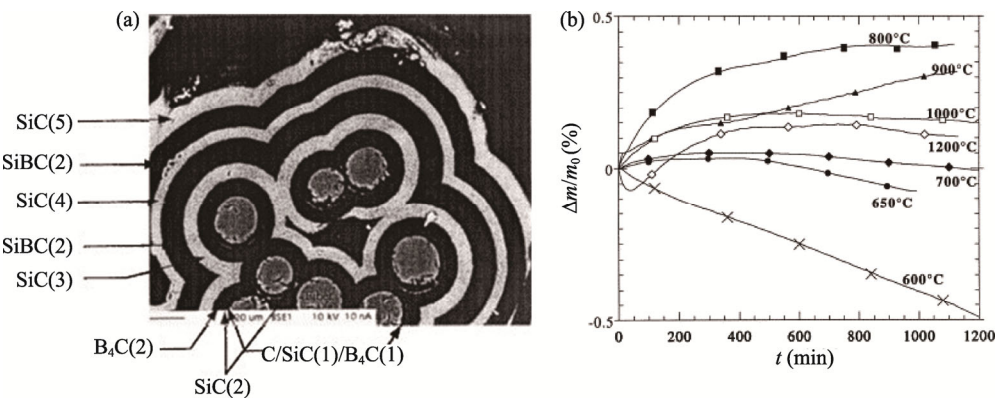

Fig. 18 (a) SEM image of the as-fabricated $SiC_f/C/(SiBC)_m$ composites; (b) weight change ($\Delta m/m_0$) vs. oxidation time (t) curves at different temperatures. Reproduced with permission from Ref. [112], © Published by Elsevier Science Ltd. 2001.

Table 3 Oxidation behaviors of $SiC_f/C/(SiBC)_m$ composites in a wet atmosphere $He–O_2(20\%)–CO_2(5\%)–H_2O(2.3\%)$ [112]

Temperature (℃)	Carbon interphase	B_4C	SiBC and SiC	Global weight change	Explanation
600	$\Delta m < 0$	$\Delta m \approx 0$	$\Delta m \approx 0$	$\Delta m < 0$ quasi-linear and continuous	No protection, calcination of the carbon interphase
650–700	$\Delta m < 0$	$\Delta m \geqslant 0$	$\Delta m \approx 0$	$\Delta m \approx 0$ weak weight change	Balance between weight loss and gain
800	$\Delta m \approx 0$ protected	$\Delta m \geqslant 0$	$\Delta m \geqslant 0$	$\Delta m \geqslant 0$	Protection of the interphase by B_2O_3
900	$\Delta m < 0$	$\Delta m \leqslant 0$ non-protective B_2O_3 film	$\Delta m \geqslant 0$	$\Delta m \geqslant 0$	Partial protection of the interphase
1000–1200	$\Delta m \approx 0$ protected	$\Delta m < 0$ volatilization	$\Delta m \geqslant 0$	$\Delta m \geqslant 0$	Protection of the interphase by silica and borosilicate

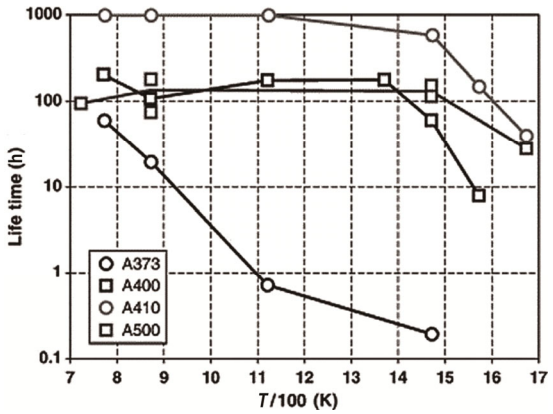

Fig. 19 Lifetime on different materials fabricateed by SNECMA of tensile fatigue tests performed at 120 MPa in air (0.25 Hz). Reproduced with permission from Ref. [114], © The American Ceramic Society 2005.

1200 ℃. It indicated that excellent duration was obtained with the design of self-healing multilayered matrix. Several kinds of CMC have been assembled in aeroengines, e.g., A262 (C/SiC) has been applied for engine outer flaps of M88-2, and A410 has been used for flame holders [5,16,113,114,117].

SiBC manufactured by the RMI was also widely studied [39,40,118–120]. The B_4C particles were used to provide the B and C elements, and SiBC was generated from the reaction between B_4C and liquid Si during the RMI process. The microstructure of RMI SiBC was different from that of SiBC by the CVI. The mechanical property and oxidation resistance ability of RMI SiBC modified C/SiC composites were further investigated. As shown in Fig. 20(a), the inner-bundle pores were filled by the CVI SiC matrix, and RMI SiBC was introduced into the inter-bundle area of C/SiC–SiBC composite. The microstructure of RMI SiBC is shown in the illustration at top right corner of Fig. 20(a). According to the X-ray diffraction (XRD) results (Fig. 20(b)), SiBC consisted of SiC (gray phase), residual Si (white phase), and $B_{12}(C,Si,B)_3$ (black phase) [121]. The oxidation behavior of C/SiC–SiBC composites was investigated in static air at the temperature range of 800–1200 ℃ for 10 h [40]. The CTE of SiBC and SiC matrix was higher than that of carbon fiber, and residual tensile stress existed in matrix when the temperature decreased from preparation temperature to room temperature. The matrix microcracks came into being because the residual tensile stress exceeded fracture stress of matrix. The matrix microcracks was open (Fig. 21(b)) because the content of borosilicate glass at the edge of microcracks was insufficient at 800 ℃. The oxidation was controlled by the diffusion rate of oxygen through matrix microcracks. The PyC interphase and carbon fiber were oxidized in Fig. 21(a). The flexural strength after oxidation at 800 ℃ correspondingly decreased. The oxidation rate of SiBC was faster, and the viscosity of borosilicate glass decreased at 1000 ℃. The matrix microcracks were partly sealed in Figs. 21(c) and 21(d), and thus oxygen diffusion channel was reduced. The carbon fiber was protected from being oxidized. The flexural strength retention ratio was enhanced with the appearance of glass phase compared with that at 800 ℃. When the oxidation temperature was increased to 1200 ℃, the matrix microcracks were fully filled by borosilicate glass (Figs. 21(e) and 21(f)). The oxidation rate was controlled by the diffusion rate of oxygen through oxide scale. The interphase and fiber were hard to be oxidized, and the flexural strength retention ratio can reach 110%. The interphase plays a significant role in relieving the residual stress in CMC, and the thickness of interphase is a meaningful control parameter. When the thickness of interphase increased from 50 to 450 nm, the residual stress decreased. The density of matrix microcracks declined from 4.76 to 3.56 mm^{-1}. The oxidation of interphase and fiber were reduced on

account of the decreased oxygen diffusion channels. The flexural strength retention ratio increased from 73% to 119% when C/SiC–SiBC was oxidized at 800 ℃ for 10 h [118]. The oxidation resistance of SiC/SiC–SiBC via the RMI was studied by Sun *et al*. [120]. The oxidation experiments were conducted at 800, 1000, and 1200 ℃ under static air for 100 h. Two kinds of SiC fiber with different compositions and CTE were chosen as the reinforcement of SiC/SiC–SiBC. The strength retention ratios of A–SiC/SiC–SiBC (with Amosic fiber as the reinforcement) after oxidation at 800, 1000, and 1200 ℃ were 109.6%, 103.2%, and 102.9%, respectively, and those of B–SiC/SiC–SiBC (with Tyranno–ZMI fiber as reinforcement) were 74.7%, 98.9%, and 104.7%, respectively. The CTE of two kinds of composites was compared with that of SiC coating from 200 to 1200 ℃. It indicated that the CTE of SiC coating was the highest. The difference of CTE between B–SiC/SiC–SiBC and SiC coating was larger and caused microcracks in SiC coating. The microcracks in SiC coating was open because the oxidation rate of SiBC was too slow to generate sufficient glass phase at 800 ℃. The oxidation of interphase and fiber occurred inside B–SiC/SiC–SiBC, and the mechanical property decreased. The flexural strength retention ratio of B–SiC/SiC–SiBC increased after oxidation at 1000 and 1200 ℃ because the borosilicate was generated rapidly and inhibited the diffusion of oxygen. The interphase and fiber were protected from oxidation. As for A–SiC/SiC–SiBC, no microcracks were observed in SiC coating, and it exhibited excellent oxidation resistance.

The results show that excellent self-healing property is obtained in SiBC-modified SiC/SiC via the CVI or RMI at 1000–1200 ℃. The borosilicate glass originating from the oxidation of SiBC plays a key role in sealing cracks, and this is consistent to our conclusion in Fig. 10. Excellent self-healing property can be obtained at wide temperature range through combined design of different self-healing components. Furthermore, it is

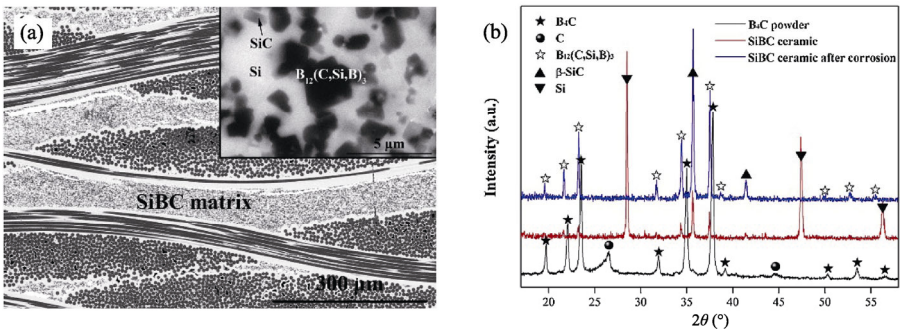

Fig. 20 (a) Backscattered electron image of C/SiC–SiBC via the RMI tenchnology; (b) XRD patterns of B_4C powders and SiBC ceramic before and after acid corrosion. Reproduced with permission from Ref. [121], © Elsevier Ltd. 2019.

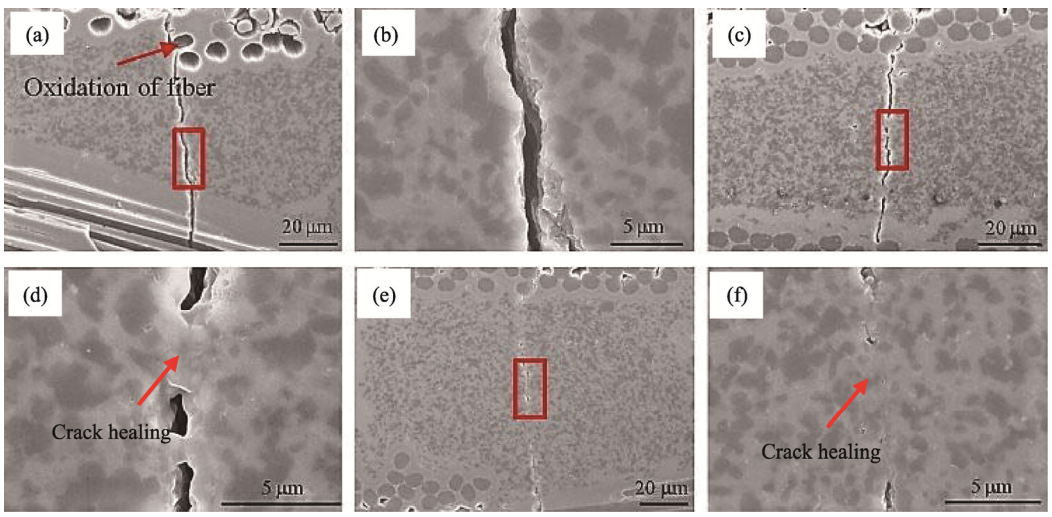

Fig. 21 Morphologies of C/SiC–SiBC composites after oxidization at (a, b) 800 ℃, (c, d) 1000 ℃, and (e, f) 1200 ℃ for 10 h. Reproduced with permission from Ref. [40], © Elsevier Ltd and Techna Group S.r.l. 2014.

worth noting that the matrix crack density can be decreased by precise microstructure design. The duration of CMC can be significantly prolonged.

4.2.3 CMC-SiC modified with SiBCN

The SiBCN ceramic with low density [122], low CTE, and excellent oxidation resistance and thermal stability (even to 2000–2200 ℃) [123–125] has been widely investigated as ceramic fiber [126–128], coating [129], and structural ceramic parts [130,131]. The oxidation behavior [132–135] and self-healing performance [99] of SiBCN were also investigated. And it is considered to be a promising material to exhibit self-healing function at 1200–1400 ℃.

At present, the oxidation resistance of SiBCN prepared by the polymer derived method and mechanical alloying (MA) is mainly studied [136]. It indicated that the pre-cracks at the surface of polymer derived SiBCN ceramic (PDC–SiBCN) can be sealed by glass phase after oxidation at 1000 ℃ for 480 min [99]. The contents of B and C elements had significant effect on the oxidation resistance of SiBCN via the MA combined with hot pressing sintering. The B_2O_3 further promoted the oxidation of SiC to produce the borosilicate glass [134]. And the oxidation resistance property was enhanced when the B element content was properly increased. Too much low melting point B_2O_3 would be generated if the content of B element is too high, and the integrity of oxide scale would be damaged with the volatilization of B_2O_3. This was harmful to the oxidation resistance. The number of holes was augmented with the addition of free carbon, and the oxidation resistance was poor [137]. However, the MA method is not a suitable method to fabricate CMC. All the following studies were about SiBCN-modified CMC via the PIP.

The wet oxidation resistance of SiBCN-modified SiC/SiC fabricated by the chemical vapor infiltration combined with polymer infiltration online pyrolysis (CVI+PIOP) process was researched by Luan *et al*. [130]. Two kinds of preforms, plain and satin weave, were chosen. The SiBCN was introduced into semi-dense SiC/SiC, and it was mainly located at inter-bundle area and homogeneously distributed in SiC matrix (Figs. 22(a) and 22(b)). The density of semi-dense plain weave SiC/SiC was adjusted. The samples with high and low contents of CVI SiC matrix were marked as DP and P, respectively, and the sample with satin weave preform was marked as S. Different oxidation temperatures (1300, 1400, and 1500 ℃) and oxidizing atmospheres (14 kPa H_2O:8 kPa O_2:78 kPa Ar, 14 kPa H_2O:20 kPa O_2:66 kPa Ar, and 30 kPa H_2O:20 kPa O_2:50 kPa Ar) were applied. After exposed for 100 h at different temperatures, both the linear segment slope (flexural modulus) and fracture load (flexural strength) of three kinds of composites decreased compared with that of the as-fabricated composites. The fracture displacement (fracture strain) increased. The pseudo plastic fracture behavior in all the samples can be observed. The property degradation of fiber and matrix after long-term oxidation also caused the decrease of mechanical property. The strength retention ratios of S and P samples decreased from 82% and 69% to 58% and 48%, respectively, with the oxidation temperature increasing from 1300 to 1500 ℃. The DP samples had the highest strength retention ratio in three kinds of samples. After oxidation at 1300 ℃ in a wet oxidation atmosphere (14 kPa H_2O:8 kPa O_2:78 kPa Ar) for 100 h, the strength retention ratio of DP samples was about 100%. With the increase of O_2 partial pressure, the flexural strength of S and P samples was essentially unchanged, and the flexural modulus slightly decreased. With the increase of H_2O partial pressure, the flexural strength and modulus of S and P slightly increased. The flexural strength of DP samples gradually decreased with the increase of O_2 partial pressure and H_2O partial pressure. The strength retention ratio of DP samples with the value of 85% was still the highest. In addition to Reactions (9), (12), (15), and (17), Reactions (20)–(23) occurred during the oxidation test:

$$2C(s) + O_2(g) \rightarrow 2CO(g) \quad (20)$$

$$4BN(s) + 3O_2(g) \rightarrow 2B_2O_3(l) + 2N_2(g) \quad (21)$$

$$2B_2O_3(l) + O_2(g) \rightarrow 4BO_2(g) \quad (22)$$

$$Si_3N_4(s) + 3O_2(g) \rightarrow 3SiO_2(s) + 2N_2(g) \quad (23)$$

The glass phases produced by the oxidation of SiBCN matrix made contribution to the high strength retention ratio. The tensile creep property of SiC/(SiC–SiBCN)$_x$ was further investigated at 1200 ℃ in an atmosphere of 12 kPa H_2O:8 kPa O_2:80 kPa Ar, and the applied stress was 90, 100, and 120 MPa [138]. The creep curves of specimens tested at 90 and 100 MPa exhibited two-stage characteristic, and one-stage behavior can be seen when tested at 120 MPa. The creep rates at the first stage were 9.48×10^{-7}, $(1.25\pm0.09)\times10^{-6}$, and $(2.95\pm0.77)\times10^{-6}$ s^{-1}, corresponding to the applied stress of 90, 100, and 120 MPa, respectively. It meant

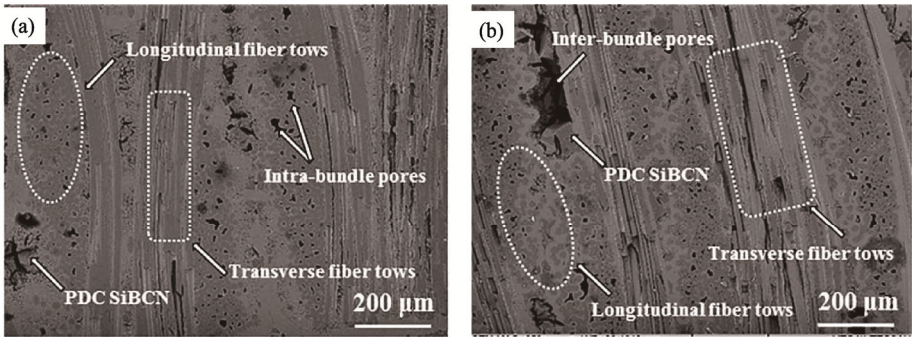

Fig. 22 Cross-section morphologies of SiC/SiC–SiBCN composites: (a) DP sample; (b) S sample. Reproduced with permission from Ref. [130], © The American Ceramic Society 2019.

that the creep rate increased with the increase of applied stress. Then, the creep rates decreased to minimum rates of about 10^{-11} and 10^{-9} s^{-1} with the increase of test time, corresponding to the applied stress of 90 and 100 MPa, respectively, which was four and three orders of magnitude smaller than that at the primary stage. The creep rate of SiC/$(SiC–SiBCN)_x$ under 90 MPa at 1200 ℃ was four orders of magnitude lower than that of Nicalon/PyC/SiC composite, and the creep life may be further enhanced. The threshold stress of creep rupture lifetime of 300 h at 1200 ℃ was about 90 MPa according to the relationship curve between the logarithm of the time to failure during creep (lg*t*) and the creep stress. The glass phase formed by the oxidation of SiBCN closed the defects, and the creep rate was decreased. The lifetime can be prolonged.

The SiBCN was also employed alone as matrix in some studies. The oxidation resistance of SiC/SiBCN via the PIP process was studied at different temperatures (800, 1000, and 1200 ℃) for 50 h in air [139]. The fracture mode changed from non-brittle to brittle after oxidation. The bending strength decreased, and the bending strength retention ratios were 35.3%, 60.3%, and 47.0% after oxidation at 800, 1000, and 1200 ℃, respectively. The fracture morphologies are shown in Fig. 23. The fiber pullout can be seen in the as-fabricated composites. The SiBCN matrix was not oxidized, and no glass phase was observed at 800 ℃. The oxygen quickly diffused into SiC/SiBCN through defects. Owing to the oxidation of BN interphase, the interface bonding strength was enhanced by B_2O_3 glass. Thus, the interface debonding and crack deflection cannot occur. After oxidation at 800 ℃ for 50 h, the fracture was flat, and no fiber pullout was observed (Fig. 23(b)). After oxidation at 1000 ℃ for 50 h, the oxidation of SiBCN was severe. Sufficient glass phase was generated, and the defects were healed. Therefore, interphase and fiber were prevented from oxidation. A small amount of pores appeared in the matrix attributed to the vaporization of glass phase (Fig. 23(c)). The bending strength retention ratio was the highest after oxidation at 1000 ℃. After oxidation at 1200 ℃ for 50 h, the oxygen diffusion rate in glass phase was high, and almost all SiBCN matrix was oxidized (Fig. 23(d)). The strength retention ratio declined. Tan *et al*. [131] also studied the oxidation resistance of SiC/SiBCN via PIP at 1350, 1500, and 1650 ℃ in air. The borosilicate glass was quickly generated and sealed the defects at all temperatures. However, the volatilization of glass phase was serious, and this made the oxide scale become thinner and porous. The oxygen would diffuse through

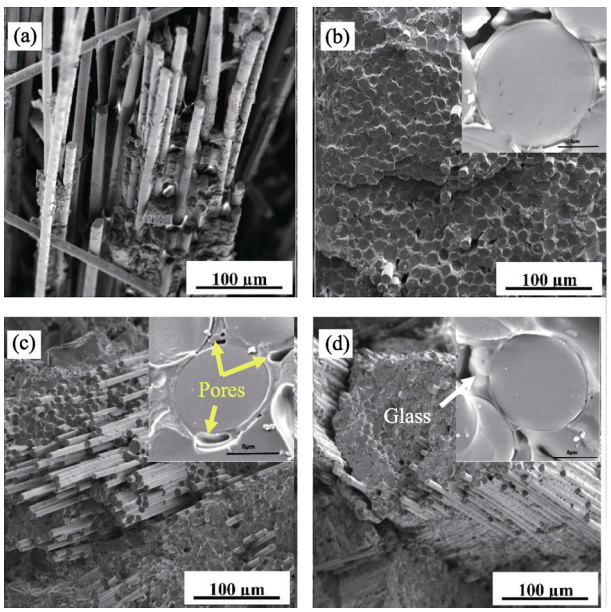

Fig. 23 SEM images of the fractured surfaces of 3D SiC_f/SiBCN composites. (a) Before oxidation treatment and after oxidation treatment at high temperatures in air for 50 h: (b) 800 ℃, (c) 1000 ℃, and (d) 1200 ℃. Reproduced with permission from Ref. [139], © Elsevier Ltd. 2020.

porous oxide scale and reacted with inner composite. The flexural strength retention ratio of SiC/SiBCN was only 54% after oxidation at 1350 ℃ for 100 h.

From the above research results, it can be seen that poor environment property is obtained when SiBCN alone acts as the matrix. As we know, SiBCN introduced into CMC is usually amorphous. SiBCN would react with oxygen when it is exposed in air at high temperatures. When the temperature is above preparation temperature, atom rearrangement and phase separate also exist in the region where oxygen cannot reach [140]. Complex reactions and residual stress field come into being in CMC. To obtain the target self-healing temperature range proposed in Fig. 10, systematic investigation is needed to be done urgently to understand the interaction between oxidation and crystallization process. And it is expected to provide the guidance for the application of SiBCN in SHCMC.

4. 3 Glass phases with high melting points for higher self-healing temperature ranges

4.3.1 Al_2O_3-stabilized glass phase

The severe volatilization of B_2O_3 (above 900 ℃), borosilicate glass (above 1200 ℃), and SiO_2 (above 1400 ℃) would destroy the integrity of oxide scale, and the inner material would be continuously oxidized. The fast diffusion rate of oxygen in oxide scale at high temperatures is also harmful to the oxidation resistance and the mechanical properties of composites. Al_2O_3 can be introduced into glass phase to improve the thermal stability and maintain the integrity of oxide scale. The transition from SiO_2 glass to cristobalite can also be avoided. Additionally, the oxygen diffusion rate is further decreased.

The beneficial effect of the addition of Al on the oxidation resistance of SiBCN was investigated [141,142]. SiBCN and SiBCNAl were manufactured. Ceramic particles with the sponge-like structure were prepared by the direct pyrolysis of the precursor without any extra processing, and SiBCN and SiBCNAl were marked as T2(1)*c* and Al3*c*, respectively. The disc-shaped samples were fabricated by warm-pressing, and SiBCN and SiBCNAl were marked as T2(1)c_{WP} and Al3c_{WP}, respectively. The oxidation experiments were conducted at 1100, 1300, and 1500 ℃ in air. After oxidation at 1500 ℃ for 100 h, the bubbles came into being at the edges of T2(1)*c* ceramic particles. The oxide scale at other areas was still dense, amorphous but full of cracks. In contrast, the oxide scale of Al3*c* was homogeneous, smooth, and free of cracks. A part of pores in sponge-like particles were covered by glass phase. The oxide scale of T2(1)c_{WP} after oxidation at 1500 ℃ for 100 h was completely bubbled, cracked, and partially peeled off. On the contrary, the oxide scale of Al3c_{WP} was dense and free of cracks or bubbles. It meant that the stability was enhanced due to the formation of mullites, aluminum borates, and Al_2O_3/B_2O_3/SiO_2 glass. Meanwhile, the fluidity of glass can be guaranteed. Shan *et al*. [86] investigated the effect of Al_2O_3 on the oxidation behavior of Si–B–C ceramic. The oxidation tests were conducted at 1200 ℃ for 98 h in different atmospheres (dry O_2 and O_2/H_2O). The results showed that the crystallization of SiO_2 glass to cristobalite was impeded with the addition of Al_2O_3, and the oxide scale was smooth and free of cracks (originating from the mismatch of CTE between SiO_2 glass and cristobalite). The addition of Al_2O_3 could weaken the tendency of bridged oxygen atoms (Si–O–Si, Si–O–Al) to become non-bridged oxygen atoms (Si–O–H). In addition, the protonated bridging oxygen (Al–O(H)–Si) acted as the linkage in the glass network. The viscosity of aluminosilicate melt was enhanced, and the reaction activity with water steam was decreased. The oxidation resistance of Si–B–C ceramic was improved.

Al_2O_3 was also introduced into SiC_f/SiC–B_4C composites to study the self-healing capacity under a wet oxygen atmosphere [143]. Pre-cracks were introduced by tensile force of 80 MPa, and the oxidation tests were performed at 1200 ℃ in an O_2/H_2O atmosphere. After oxidation for 5 h, the cracks in matrix were sealed by glass phase. The cracks in the fiber region were still not completely sealed even after 50 h for virgin composite. In contrast, the cracks in both matrix area and fiber area of composites with 15% Al_2O_3 were fully healed by glass phase after exposure for 5 h. The cracks were still healed after oxidation for 50 h due to the excellent thermal stability of glass phase with the addition of Al_2O_3. The BN interphase and SiC fiber were partially oxidized in all composites. However, the dissolution of Al_2O_3 in glass phase increased the viscosity of glass phase and decreased the diffusion rate of oxygen in the glass phase. The oxidation of BN interphase and SiC fiber in Al_2O_3-modified composites was slighter. It made great contribution to the mechanical property of composites. The tensile strength retention ratio of Al_2O_3-modified

composites increased 10.8% and 18.8% compared with virgin composites after oxidizing 10 and 50 h, respectively. The oxidation test was also performed at 1100 ℃ for 200 h in an O_2/H_2O atmosphere [144]. The evolution of morphology and mechanical property was obtained. The surface morphology differences of virgin and Al_2O_3-modified $SiC_f/SiC–B_4C$ composites can be seen after oxidation (Fig. 24). For virgin composites, the cracks existed on the surface of fiber after oxidation for 100 h or even for 200 h (Fig. 24(b)). The continuous oxidation damage of the internal material occurred because the oxygen diffused into composites through open cracks. Only small amount of cracks on the fiber surface can be observed in Al_2O_3-modified $SiC_f/SiC–B_4C$ composites. Smooth and dense oxide scale was formed on the surface of Fig. 24(d). The oxygen was hindered outside the composites with the addition of Al_2O_3. The penetration depth of oxygen in Al_2O_3-modified composites (10–20 μm) further decreased compared with virgin composites (40–60 μm) (Figs. 24(e) and 24(f)). The mechanical property was obtained by three-point bending test, and the AE technique was also employed to monitor the damage process during three-point bending test. As for Al_2O_3-modified specimens, the retentions of σ_{min} (first AE stress, formation of microcrack) and σ_{onset} (AE onset stress, the large or transverse matrix cracks propagating at the through-thickness direction) oxidized for 100 h increased 9.46%±7.71% and 7.74%±6.08% compared with virgin composites, respectively. When the oxidation time increased to 200 h, the retention of σ_{min} and σ_{onset} even increased 19.22%±6.33% and 15.14%±6.01%, respectively. It meant that the interior material was protected from oxidation by dense and smooth oxide layer with the addition of Al_2O_3. The excellent surface without cracks made great contribution to the improvement of matrix cracking stress. The above studies provide a favorable theoretical guidance for the wide application of Al_2O_3 in SHCMC.

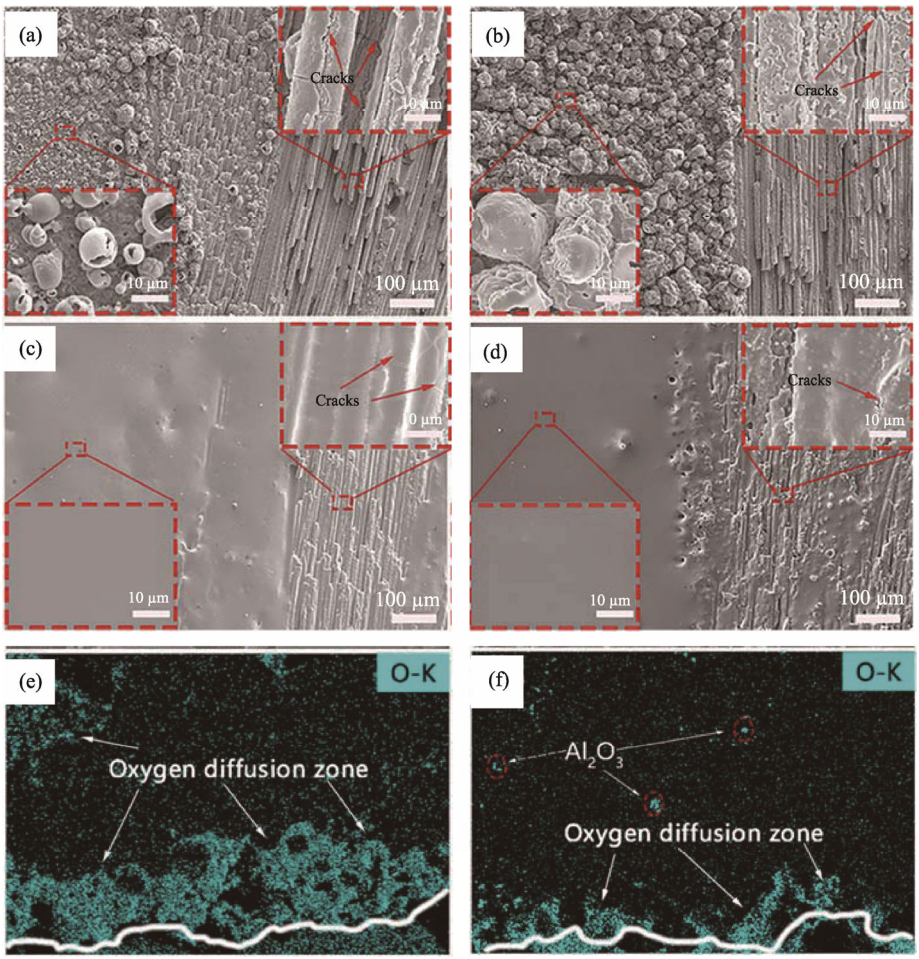

Fig. 24 SEM images of the surface of the $SiC_f/SiC–B_4C$ sample after oxidation for 100 h: (a) with 0% Al_2O_3, (c) with 15% Al_2O_3; for 200 h: (b) with 0% Al_2O_3, (d) with 15% Al_2O_3; O distributions in $SiC_f/SiC–B_4C$: (e) with 0% Al_2O_3, (f) with 15% Al_2O_3. Reproduced with permission from Ref. [144], © WILEY-VCH Verlag GmbH & Co. KGaA, Weinheim 2019.

4.3.2 ZrO_2–SiO_2 and HfO_2–SiO_2 glass

Similar to SiO_2–B_2O_3 glass, the eutectic temperature also exists in ZrO_2–SiO_2 and HfO_2–SiO_2 system, which is lower than the melting point of ZrO_2 and HfO_2 or SiO_2 because both ZrO_2 and HfO_2 can dissolve in SiO_2 glass. Therefore, the viscosity and stability of SiO_2 are enhanced. The diffusion rate of oxygen in oxide scale is accordingly decreased. It is expected that the self-healing capacity of ZrO_2- or HfO_2-modified CMC can be improved above 1400 ℃.

The SiBCNZr ceramic was prepared by the sol–gel method combined with reactive spark plasma sintering (SPS) process, and the oxidation behavior was studied [145–147]. ZrB_2, SiC, and BN(C) phases existed in the as-fabricated SiBCNZr ceramic. The surface was slightly oxidized after the SiBCNZr ceramic was exposed at 1500 ℃ for 1 h in air. The B_2O_3, SiO_2, and ZrO_2 were produced by the oxidation of SiBCNZr. With the increase of oxidation time, the surface became rougher. The glass phase appeared on the surface after oxidation for 3 h. Then the surface was fully covered by glass phase with the increase of oxidation time, meanwhile, many pores existed in oxide scale. The pores might come from the vaporization of B_2O_3. The inner material was further oxidized because the oxygen quickly diffused through the pores. The appearance of $ZrSiO_4$ by the reaction between ZrO_2 and SiO_2 also hindered the volatilization of SiO_2 and decreased the diffusion rate of oxygen [148,149]. The oxidation resistance of SiBCNZr was effectively improved. The SiBCN/ZrB_2–ZrN ceramics can also be fabricated by the MA combined with reactive hot press sintering, and the oxidation experiments were conducted in the following air (N_2 79%, O_2 21%, steam content < 50 ppm) at 1100, 1200, 1300, and 1500 ℃ for 5 h [150]. The main crystals were ZrB_2, ZrN, and SiC, and a small amount of BNC and ZrO_2 also existed in SiBCN/ZrB_2–ZrN ceramics. The $ZrSiO_4$, SiO_2, and ZrO_2 phases appeared after oxidation according to the XRD patterns. The diffraction peak intensity of $ZrSiO_4$ increased with the rise of oxidation temperature. The glass phase covered the surface of ceramics after oxidation at 1100 ℃ for 5 h. The SiO_2 glass showed liquid and amorphous characteristics, and $ZrSiO_4$ crystal appeared in amorphous SiO_2 as an island structure. The morphology of the samples after oxidized at 1500 ℃ for 5 h showed that the $ZrSiO_4$ with the size of 20 μm was uniformly distributed in SiO_2 glass (Fig. 25(a)). In addition to Reactions (15) and (22), Reactions (25)–(27) may occur during oxidation:

$$2ZrN(s) + 2O_2(g) \rightarrow 2ZrO_2(l) + N_2(g) \quad (25)$$

$$2ZrB_2(s) + 5O_2(g) \rightarrow 2ZrO_2(l) + 2B_2O_3(l) \quad (26)$$

$$SiC(s) + O_2(g) \rightarrow SiO(g) + CO(g) \quad (27)$$

According to the SiO_2–ZrO_2 phase diagram (Fig. 26(b)), $ZrSiO_4$ was formed by the reaction between SiO_2 and ZrO_2. Meanwhile, the eutectic temperature (1687 ℃) [92] existed in SiO_2–ZrO_2 system similar to SiO_2–B_2O_3 system. With the solution of ZrO_2 in SiO_2 glass, the SiO_2–ZrO_2 glass came into being. The vaporization of SiO_2 glass was prevented, and the viscosity of ZrO_2 was decreased [85,148,151]. SiO_2–ZrO_2 glass may achieve our desired self-healing function above 1400 ℃.

Ouyang *et al*. [152] employed ZrB_2–SiO_2 as self-healing coating to improve the oxidation resistance of SiC-coated C/C composites. A ZrB_2 porous skeleton

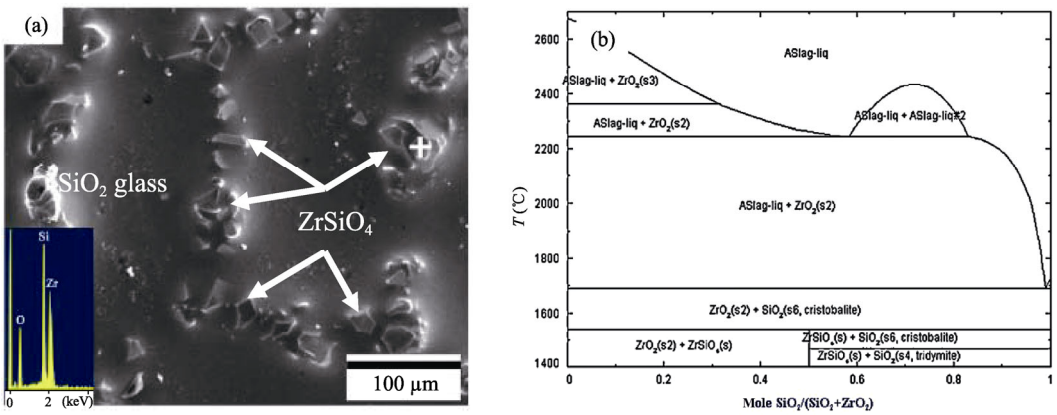

Fig. 25 (a) Surface morphology of SiBCN/ZrB_2–ZrN ceramic after oxidation at 1100 ℃ for 5 h; (b) SiO_2–ZrO_2 phase diagram. Reproduced with permission from Ref. [150], © Elsevier Ltd. 2015.

layer was firstly prepared on the surface of composites by the hydrothermal electrophoretic deposition method. Then, the samples were infiltrated in silica sol. The SiO_2 filled the pores between ZrB_2 particles after drying at 50 ℃ and heated at 800 ℃. The morphology and phase composition were recorded during oxidation at 1500 ℃ for 330 h. After oxidation for 3 h, ZrB_2, ZrO_2, and SiO_2 appeared. The ZrO_2 was the oxidation product of ZrB_2, and another product of B_2O_3 cannot be detected by the XRD. The surface of composites was covered by glass, and micro-scale particles can also be observed in glass phase (Fig. 26(a)). According to the EDS results, the glass phase was borosilicate glass, and the particles were ZrO_2. When the oxidation time increased to 210 h, the $ZrSiO_4$ also appeared in addition to ZrO_2 and SiO_2. The coating was still free of cracks and covered by glass. Many particles with a size of 1–2 μm embedded in glass phase, as shown in Fig. 26(b). According to the EDS results, the glass phase was SiO_2, and the particles were $ZrSiO_4$. Many wrinkles were formed in the coating with the formation of compressive stress. The compressive stress can be attributed to volume expansion. On one hand, the solid phase transformation during oxidation process made great contribution to compressive stress. The volume expansion is 13.6% and 98% with the conversion of ZrB_2 to ZrO_2 and ZrO_2 to $ZrSiO_4$, respectively. On the other hand, the volume expansion is 5% combined with the phase transition of ZrO_2 from tetragonal phase to monoclinic phase during cooling. The compressive stress can restrain the formation of cracks. After oxidation for 330 h, only $ZrSiO_4$ and SiO_2 can be detected. The compressive stress caused by volume expansion was relived owing to the flow of glass phase. Cracks came into being because of the CTE mismatch between coating and substrate, as shown in Fig. 26(c). The inner material would be further oxidized with the formation of bubbles. It indicated that little research has been done on self-healing property of ZrO_2–SiO_2 glass. The self-healing mechanism and characteristic is unclear. Extensive experiments and in-depth studies are required in the self-healing property of ZrO_2–SiO_2 glass.

Similar to the SiO_2–ZrO_2 system, SiO_2 can also react with HfO_2 to form $HfSiO_4$, and the $SiCO_x$–HfO_2–$HfSiO_4$ glass system came into being [153]. The Hf-modified polyborosilazanes (PBSZHf) was manufactured, and SiBCN/HfN ceramics were fabricated by cross-linking and pyrolysis of as-fabricated precursor. The oxidation resistance property was studied at the temperature range of 1100–1500 ℃ in air. The SiO_2 and HfO_2 formed after oxidation at 1100–1500 ℃, and $HfSiO_4$ was generated at 1500 ℃ according to the EDS results. The eutectic temperature (1680 ℃) also existed in the SiO_2–HfO_2 system [92,94]. The SiO_2–HfO_2 glass phase modified with $HfSiO_4$ effectively protected the inner material from further oxidation.

Luan *et al*. [154] fabricated C/SiC–SiHfBCN composites by the CVI combined with the PIOP process. The oxidation resistance was researched at 1200–1400 ℃ for 50 h in a wet oxygen atmosphere. The glass covered the surface of composites after oxidation. The diffraction peaks belonging to SiO_2, HfO_2, and $HfSiO_4$ appeared in the XRD curves. The bending strength retention ratio decreased with the increase of oxidation temperature and partial pressure of O_2 and H_2O. With the increase of O_2 and H_2O partial pressure, the bending strength retention ratio was 85% after oxidation at 1300 ℃. After oxidation at 1400 ℃ for 50 h, the bending strength retention ratio was about 75%. The $HfSiO_4$ produced by the reaction between SiO_2 and HfO_2 was also a kind of glass phase [155], and the viscosity and thermal stability of which were higher than those of SiO_2. The cracks can be healed by SiO_2–HfO_2 combined with $HfSiO_4$ glass, and the self-healing property was enhanced.

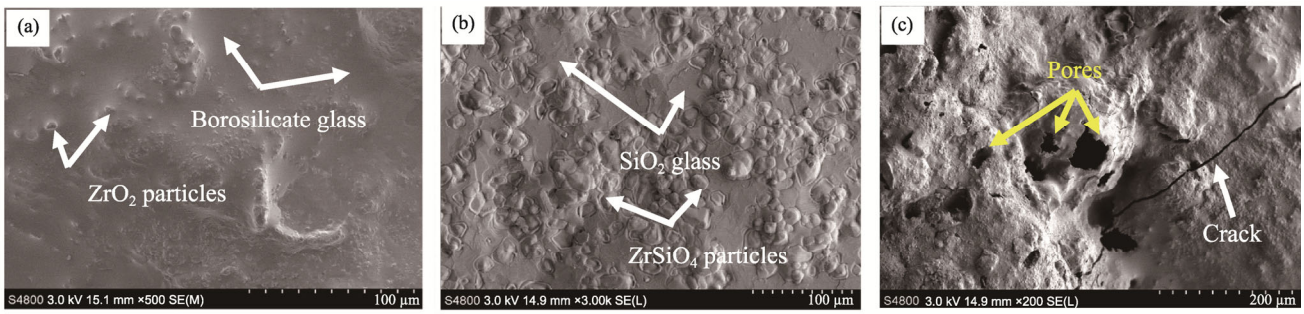

Fig. 26 Surface morphologies of the ZrB_2–SiO_2 coating on SiC-coated C/C composites after oxidation at 1500 ℃ for (a) 3 h, (b) 210 h, and (c) 330 h. Reproduced with permission from Ref. [152], © Elsevier Ltd. 2016.

It is worth noting that much attention is paid to the ablation resistance property of Zr- or Hf-containing compound modified C/C composites [88,89,156–159]. The self-healing property has not attracted much attention. According to the phase diagrams, the eutectic temperatures of SiO_2–ZrO_2 and SiO_2–HfO_2 system are high. The effective self-healing temperatures of SiO_2–ZrO_2 and SiO_2–HfO_2 may be much higher than the working temperatures of some types of SiC fiber (below 1300 ℃). Furthermore, whether the generation rate of SiO_2–ZrO_2 and SiO_2–HfO_2 glass is fast enough to seal the cracks is also worth pondering. Much research work will have to be done before ZrO_2 and HfO_2 are applied in SHCMC.

5 Conclusions

Long-term CMC, which can serve at thermo-mechanical-oxygenic coupling environment for hundreds and even thousands of hours, usually shows several key characteristics, including high degree of densification, high σ_{mc}, and containing self-healing components or two of them. The pores in CMC act as crack source and promote the initiation of matrix cracks at low loads. In addition, the pores provide diffusion pathway for oxygen, and it is harmful to self-healing performance. Thus, the high degree of densification is the basic characteristic for CMC to obtain high σ_{mc} and excellent self-healing property.

Structure design, component selection, and technological control should be taken into account for long-duration CMC. The structural design mainly includes four aspects, namely fiber preform structure, interface shear strength, CTE match between fiber and matrix, and matrix strengthening. The fiber preform architecture, which has the characteristic of high fiber volume fraction in loading direction and low fiber volume fraction perpendicular to the loading direction, is chosen to ensure the excellent mechanical property. The higher interface shear strength is designed to ensure good load transfer capacity from matrix to fiber. Meanwhile, the interface debonding and crack deflection should be ensured to occur. The residual compressive stress can be applied to matrix in axial direction by using SiC fiber with higher CTE than that of SiC matrix, and thus the applied tensile stress is partially offset. The strong matrix can be obtained by introducing the nano-scale reinforcement into matrix. On the one hand, σ_{mc} can be improved by structure design, and the crack initiation is delayed. On the other hand, the matrix crack density and crack width are designed to be decreased to decline the oxygen diffusion pathway.

According to the effective self-healing temperature range of different self-healing components, the matrix composition is highly designable for specific service environment. The self-healing component, which possesses suitable initial oxidation temperature and high oxidation rate and generates stable glass phase at service environment, is preferred for specific service temperature. Furthermore, the matrix composition can be designed with multiple self-healing components to meet the requirement for a wide self-healing temperature range. Distance to fiber from far to near, the initial oxidation temperature of self-healing components should be lower and lower, and the oxidation rate should be faster and faster. When the CMC is loaded, the microcracks initiate and propagate in matrix. Oxygen diffuses along microcracks, and it can be partly consumed by the outer self-healing component. The microcracks can be partially healed by the produced glass phase. With the propagation of matrix microcracks, the inner self-healing components with a high oxidation rate are quickly oxidized and produce sufficient glass phase to seal the microcracks. The interphase and fiber can be protected from oxidation resulting from the gradual consumption of oxygen by multiple self-healing components when the cracks propagate from the external to the interior. The location of the glass phase with a low melting point is far from the surface, and the evaporation of which is further hindered by outer high melting point glass phase. The excellent self-healing property can be obtained, and the service life is obviously prolonged.

The last question is the process technology to achieve target structure and compositions. Though there are several kinds of technologies to fabricate CMC, some methods may cause damage to CMC components. Both the damage of preparation temperature to SiC fiber and the erosion of liquid Si or active free radicals to interphase and fiber should be prevented.

With the development of aeronautical and space engines, the service condition of thermal-structure components would be more and more severe. The higher service stress and temperature put higher demands on the mechanical property and self-healing performance of CMC. The SHCMC would be a kind of key thermal-

structure material to meet future demand of high thrust-to-weight ratio engine, which also possesses high degree of densification or high σ_{mc} characteristic. Al-, Hf-, or Zr-modified SiBCN ceramics, which could generate glass phase with higher melting point after oxidation, are potential self-healing components for higher self-healing temperatures. In addition, the investigation on the wet-oxygen resistance of interphase and matrix is being done to reduce the dependence on the EBC during the long service period. Currently, the performance database of CMC is urgently needed to be built to provide basic data for structure and composition design. In addition, it is meaningful to develop the modeling tool to monitor the damage evolution and predict the life of CMC.

Acknowledgements

This work was supported by the National Natural Science Foundation of China (Grant Nos. 92060202, 51632007, 51872229, and 51521061), the 111 Project of China (Grant No. B08040), and National Science and Technology Major Project (Grant No. 2017-VI-0007-0077).

References

[1] Dicarlo JA, Yun HM, Morscher GN, *et al*. Progress in SiC/SiC composites for engine applications. In: *High Temperature Ceramic Matrix Composites*. Krenkel W, Naslain R, Schneider H, Eds. Weinheim, Germany: Wiley-VCH Verlag GmbH & Co. KGaA, 2001: 777–782.

[2] Naslain RR, Pailler RJF, Lamon JL. Single- and multilayered interphases in SiC/SiC composites exposed to severe environmental conditions: An overview. *Int J Appl Ceram Technol* 2010, **7**: 263–275.

[3] Naslain RR. SiC-matrix composites: Nonbrittle ceramics for thermo-structural application. *Int J Appl Ceram Technol* 2005, **2**: 75–84.

[4] Dicarlo JA, van Roode M. Ceramic composite development for gas turbine engine hot section components. In: Proceedings of the ASME Turbo Expo 2006: Power for Land, Sea, and Air, Barcelona, Spain, 2008: 221–231.

[5] Christin F. Design, fabrication, and application of thermostructural composites (TSC) like C/C, C/SiC, and SiC/SiC composites. *Adv Eng Mater* 2002, **4**: 903–912.

[6] Pierce JL, Zawada LP, Srinivasan R. Tensile properties of nicalon fiber-reinforced carbon following aerospace turbine engine testing. *J Mater Eng Perform* 2003, **12**: 354–362.

[7] Staehler JM, Zawada LP. Performance of four ceramic-matrix composite divergent flap inserts following ground testing on an F110 turbofan engine. *J Am Ceram Soc* 2004, **83**: 1727–1738.

[8] Cavalier JC, Berdoyes I, Bouillon E. Composites in aerospace industry. *Advances in Sci & Tech* 2006, **50**: 153–162.

[9] Boyle RJ, Parikh AH, Nagpal VK, *et al*. Ceramic matrix composites for high pressure turbine vanes. In: Proceeding of the ASME Turbo Expo 2014: Turbine Technical Conference and Exposition, Düsseldorf, Germany, 2014, GT2014-27136, V006T02A013.

[10] Grujicic M, Snipes J, Yavari R, *et al*. Computational investigation of foreign object damage sustained by environmental barrier coatings (EBCs) and SiC/SiC ceramic-matrix composites (CMCs). *Multidiscip Modeling Mater Struct* 2015, **11**: 238–272.

[11] Liu QM, Huang SZ, He AJ. Research progress in environmental barrier coatings of SiC ceramic matrix composites. *J Mater Eng* 2018, **46**: 1–8. (in Chinese)

[12] Lu YH, Wang YG. Formation and growth of silica layer beneath environmental barrier coatings under water-vapor environment. *J Alloys Compd* 2018, **739**: 817–826.

[13] Heveran CM, Xu JP, Sarin VK, *et al*. Simulation of stresses in TBC–EBC coating systems for ceramic components in gas turbines. *Surf Coat Technol* 2013, **235**: 354–360.

[14] Lee KN. Current status of environmental barrier coatings for Si-based ceramics. *Surf Coat Technol* 2000, **133–134**: 1–7.

[15] Naslain R. Challenging ceramic matrix composites for applications in severe environments. *Adv Compos Mater* 1995, **5**: 35–44.

[16] Cavalier J C, Berdoyes I, Bouillon E. Composites in aerospace industry. *Adv Sci Technol* 2006, **50**: 153–162.

[17] Yun HM, Dicarlo JA, Bhatt RT, *et al*. Processing and structural advantages of the Sylramic-iBN SiC fiber for SiC/SiC components. In: *the 27th Annual Cocoa Beach Conference on Advanced Ceramics and Composites: B: Ceramic Engineering and Science Proceedings*, *Volume 24*. Kriven WM, Lin HT, Eds. Westerville, USA: The American Ceramic Society 735 Ceramic Place, 2003: 247–253.

[18] Naslain R, Langlais F, Fedou R. The CVI-processing of ceramic matrix composites. *J Phys Colloques* 1989, **50**: C5-191–C5-207. (in French)

[19] Yin XW, Cheng LF, Zhang LT, *et al*. Fibre-reinforced multifunctional SiC matrix composite materials. *Int Mater Rev* 2017, **62**: 117–172.

[20] Mingazzini C, Brentari A, Burgio F, *et al*. Optimization of a pyrolysis procedure for obtaining SiC–SiC_f CMC by PIP for thermostructural applications. *Adv Sci Technol* 2013, **77**: 153–158.

[21] Jiang JM, Wang S, Li W, *et al*. Preparation of 3D C_f/ZrC–SiC composites by joint processes of PIP and RMI. *Mater Sci Eng A* 2014, **607**: 334–340.

[22] Naslain RR. SiC-matrix composites: Nonbrittle ceramics for thermo-structural application. *Int J Appl Ceram Technol* 2005, **2**: 75–84.

[23] Cheng LF, Wu SJ, Zhang LT, *et al*. Mechanical

self-adaptability of a SiC/PyC/SiC composite during oxidation in air. *J Compos Mater* 2009, **43**: 305–313.

[24] Cheng LF, Xu YD, Zhang LT, *et al*. Effect of carbon interlayer on oxidation behavior of C/SiC composites with a coating from room temperature to 1500 ℃. *Mater Sci Eng A* 2001, **300**: 219–225.

[25] Wang HL, Gao ST, Peng SM, *et al*. KD-S SiC_f/SiC composites with BN interface fabricated by polymer infiltration and pyrolysis process. *J Adv Ceram* 2018, **7**: 169–177.

[26] Bansal NP, Eldridge JI. Hi-Nicalon fiber-reinforced celsian matrix composites: Influence of interface modification. *J Mater Res* 1998, **13**: 1530–1537.

[27] Hillig WB. Strength and toughness of ceramic matrix composites. *Annu Rev Mater Sci* 1987, **17**: 341–383.

[28] Rebillat F. *Advances in Ceramic Matrix Composites*, 2nd edn. Cambridge, UK: Woodhead Publishing, 2014.

[29] Goujard S, Vandenbulcke L, Tawil H. The oxidation behaviour of two- and three-dimensional C/SiC thermostructural materials protected by chemical-vapour-deposition polylayers coatings. *J Mater Sci* 1994, **29**: 6212–6220.

[30] Goujard S, Vandenbulcke L, Tawil H. Oxidation behavior of 2D and 3D carbon/carbon thermostructural materials protected by CVD polylayer coatings. *Thin Solid Films* 1994, **252**: 120–130.

[31] Ruggles-Wrenn MB, Pope MT. Creep behavior in interlaminar shear of a SiC/SiC ceramic composite with a self-healing matrix. *Appl Compos Mater* 2014, **21**: 213–225.

[32] Lamouroux F, Bertrand S, Pailler R, *et al*. Oxidation-resistant carbon-fiber-reinforced ceramic-matrix composites. *Compos Sci Technol* 1999, **59**: 1073–1085.

[33] Lamouroux F, Bertrand S, Pailler R, *et al*. A multilayer ceramic matrix for oxidation resistant carbon fibers-reinforced CMCs. *Key Eng Mater* 1999, **164–165**: 365–368.

[34] Luan XG, Zou Y, Hai XH, *et al*. Degradation mechanisms of a self-healing $SiC_{(f)}/BN_{(i)}/[SiC–B_4C]_{(m)}$ composite at high temperature under different oxidizing atmospheres. *J Eur Ceram Soc* 2018, **38**: 3804–3813.

[35] Zuo XZ, Zhang LT, Liu YS, *et al*. Oxidation behaviour of two-dimensional C/SiC modified with self-healing Si–B–C coating in static air. *Corros Sci* 2012, **65**: 87–93.

[36] Forio P, Lamon J. Fatigue behavior at high temperatures in Air of a 2D SiC/Si–B–C composite with a self-healing multilayered matrix. In: *Advances in Ceramic Matrix Composites VII, Volume 28*. Bansal NP, Singh J, Lin HT, Eds. Indianapolis, USA: The American Ceramic Society, 2012: 127–141.

[37] Quemard L, Rebillat F, Guette A, *et al*. Self-healing mechanisms of a SiC fiber reinforced multi-layered ceramic matrix composite in high pressure steam environments. *J Eur Ceram Soc* 2007, **27**: 2085–2094.

[38] Zhang Q, Zuo XZ, Liu YS, *et al*. Oxidation behaviors and mechanisms of CVD Si–B–C ceramic in wet oxygen from 700 ℃ to 1400 ℃. *J Eur Ceram Soc* 2016, **36**: 3709–3715.

[39] Cao XY, Yin XW, Fan XM, *et al*. High-temperature flexural properties of SiBC modified C/SiC composites. *Ceram Int* 2014, **40**: 6185–6190.

[40] Cao XY, Yin XW, Ma XK, *et al*. Oxidation behavior of SiBC matrix modified C/SiC composites with different PyC interphase thicknesses. *Ceram Int* 2015, **41**: 1695–1700.

[41] Goujard S, Vandenbulcke L, Tawil H. Oxidation tests of carbonaceous composite materials protected by Si–B–C CVD coatings. *Thin Solid Films* 1994, **245**: 86–97.

[42] Luan XG, Wang L, Zou Y, et al. Oxidation behavior of C/SiC–SiBCN composites at high temperature. *J Eur Ceram Soc* 2019, **39**: 3003–3012.

[43] Vandenbulcke L, Fantozzi G, Goujard S, *et al*. Outstanding ceramic matrix composites for high temperature applications. *Adv Eng Mater* 2005, **7**: 137–142.

[44] Hatta H, Sohtome T, Sawada Y, *et al*. High temperature crack sealant based on SiO_2–B_2O_3 for SiC coating on carbon–carbon composites. *Adv Compos Mater* 2003, **12**: 93–106.

[45] Han WB, Hu P, Zhang XH, *et al*. High-temperature oxidation at 1900 ℃ of ZrB_2–*x*SiC ultrahigh-temperature ceramic composites. *J Am Ceram Soc* 2008, **91**: 3328–3334.

[46] Han JC, Hu P, Zhang XH, *et al*. Oxidation-resistant ZrB_2–SiC composites at 2200 ℃. *Compos Sci Technol* 2008, **68**: 799–806.

[47] Rezaie A, Fahrenholtz WG, Hilmas GE. Evolution of structure during the oxidation of zirconium diboride–silicon carbide in air up to 1500 ℃. *J Eur Ceram Soc* 2007, **27**: 2495–2501.

[48] Lavrenko VO, Panasyuk AD, Grigorev OM, *et al*. High-temperature oxidation of ZrB_2–SiC and ZrB_2–SiC–$ZrSi_2$ ceramics up to 1700 ℃ in air. *Powder Metall Met Ceram* 2012, **51**: 217–221.

[49] Wang PP, Tong MD, Wang HH, *et al*. Gradient HfB_2–SiC multilayer oxidation resistant coating for C/C composites. *Ceram Int* 2018, **44**: 20968–20973.

[50] Bhatt RT, Choi SR, Cosgriff LM, *et al*. Impact resistance of uncoated SiC/SiC composites. *Mater Sci Eng A* 2008, **476**: 20–28.

[51] Brewer D. HSR/EPM combustor materials development program. *Mater Sci Eng A* 1999, **261**: 284–291.

[52] Dicarlo JA, Yun HM, Morscher GN, *et al*. Progress in SiC/SiC ceramic composite development for gas turbine hot-section components under NASA EPM and UEET programs. In: Proceedings of the ASME Turbo Expo 2002: Power for Land, Sea, and Air, Amsterdam, the Netherlands, 2009: 39–45.

[53] Dicarlo JA. Advances in SiC/SiC composites for aero-propulsion. NASA/TM—2013-217889.

[54] Dicarlo JA, Yun HM, Morscher GN, *et al*. SiC/SiC Composites for 1200 ℃ and above. In: *Handbook of Ceramic Composites*. Narottam PB, Ed. Boston, USA: Springer New York, 2005: 77–98.

[55] Dicarlo JA, Yun HM, Hurst JB. Fracture mechanisms for

SiC fibers and SiC/SiC composites under stress-rupture conditions at high temperatures. *Appl Math Comput* 2004, **152**: 473–481.

[56] Lang J, Dicarlo JA. Further developments in modeling creep effects within structural SiC/SiC components. In: Peoceedings of the 32nd Annual Conference Composites Materials and Structures, Daytona Beach, USA, 2008: 20080047429.

[57] Bhatt RT, Dicarlo JA, Mccue TR. Thermal stability of melt infiltrated SiC/SiC composites. In: *27th Annual Cocoa Beach Conference on Advanced Ceramics and Composites: B: Ceramic Engineering and Science Proceedings*, *Volume 24*. Kriven WM, Lin HT, Eds. Westerville, USA: The American Ceramic Society 735 Ceramic Place, 2003: 295–300.

[58] Dicarlo JA, Bhatt RT, Mccue TR. Modeling the thermostructural stability of melt infiltrated SiC/SiC composites. In: *27th Annual Cocoa Beach Conference on Advanced Ceramics and Composites: B: Ceramic Engineering and Science Proceedings*, *Volume 24*. Kriven WM, Lin HT, Eds. Westerville, USA: The American Ceramic Society 735 Ceramic Place, 2003: 465–470.

[59] Shimoda K, Hinoki T, Katoh Y, *et al*. Development of the tailored SiC/SiC composites by the combined fabrication process of ICVI and NITE methods. *J Nucl Mater* 2009, **384**: 103–108.

[60] Dong SM, Katoh Y, Kohyama A. Processing optimization and mechanical evaluation of hot pressed 2D Tyranno-SA/SiC composites. *J Eur Ceram Soc* 2003, **23**: 1223–1231.

[61] Katoh Y, Dong SM, Kohyama A. Thermo-mechanical properties and microstructure of silicon carbide composites fabricated by nano-infiltrated transient eutectoid process. *Fusion Eng Des* 2002, **61–62**: 723–731.

[62] Park JS, Jung HC, Ooi Y, *et al*. Fabrication of environmentally resistant NITE-SiC/SiC composites. *IOP Conf Ser Mater Sci Eng* 2011, **18**: 202012.

[63] Sigl LS, Evans AG. Effects of residual stress and frictional sliding on cracking and pull-out in brittle matrix composites. *Mech Mater* 1989, **8**: 1–12.

[64] Morscher GN, Gregory N. Matrix cracking in four different 2D SiC/SiC composite systems. In: Proceedings of the 35th International SAMPE Technical Conference, Dayton, USA, 2003: 20040031565.

[65] Morscher GN, Yun HM, Dicarlo JA. Matrix cracking in 3D orthogonal melt-infiltrated SiC/SiC composites with various *Z*-fiber types. *J Am Ceram Soc* 2005, **88**: 146–153.

[66] Morscher GN, Yun HM, Dicarlo JA. In-plane cracking behavior and ultimate strength for 2D woven and braided melt-infiltrated SiC/SiC composites tensile loaded in off-axis fiber directions. *J Am Ceram Soc* 2007, **90**: 3185–3193.

[67] Morscher GN, Dicarlo JA, Kiser JD, *et al*. Effects of fiber architecture on matrix cracking for melt-infiltrated SiC/SiC composites. *Int J Appl Ceram Technol* 2010, **7**: 276–290.

[68] Li LB. Synergistic effects of temperature and oxidation on matrix cracking in fiber-reinforced ceramic-matrix composites. *Appl Compos Mater* 2017, **24**: 691–715.

[69] Li LB. Modeling matrix multicracking development of fiber-reinforced ceramic-matrix composites considering fiber debonding. *Int J Appl Ceram Technol* 2019, **16**: 97–107.

[70] Naslain RR. The design of the fibre-matrix interfacial zone in ceramic matrix composites. *Compos A Appl Sci Manuf* 1998, **29**: 1145–1155.

[71] Cook J, Gordon JE. A mechanism for the control of crack propagation in all-brittle systems. *Proc Roy Soc A Math Phys Eng Sci* 1964, **282**: 508–520.

[72] Pompidou S, Lamon J. Analysis of crack deviation in ceramic matrix composites and multilayers based on the Cook and Gordon mechanism. *Compos Sci Technol* 2007, **67**: 2052–2060.

[73] Ma XK, Yin XW, Cao XY, *et al*. Effect of heat treatment on the mechanical properties of SiC_f/BN/SiC fabricated by CVI. *Ceram Int* 2016, **42**: 3652–3658.

[74] Lowden RA, More KL. The effect of fiber coatings on interfacial shear strength and the mechanical behavior of ceramic composites. *MRS Proc* 1989, **170**: 205–214.

[75] Zhu GX, Xue YD, Hu JB, *et al*. Influence of boron nitride nanotubes on the damage evolution of SiC_f/SiC composites. *J Eur Ceram Soc* 2018, **38**: 4614–4622.

[76] Feng W, Zhang LT, Liu YS, *et al*. The improvement in the mechanical and thermal properties of SiC/SiC composites by introducing CNTs into the PyC interface. *Mater Sci Eng A* 2015, **637**: 123–129.

[77] Morscher GN, Singh M, Kiser JD, *et al*. Modeling stress-dependent matrix cracking and stress–strain behavior in 2D woven SiC fiber reinforced CVI SiC composites. *Compos Sci Technol* 2007, **67**: 1009–1017.

[78] Bunsell AR, Piant A. A review of the development of three generations of small diameter silicon carbide fibres. *J Mater Sci* 2006, **41**: 823–839.

[79] Pavia F, Letertre A, Curtin WA. Prediction of first matrix cracking in micro/nanohybrid brittle matrix composites. *Compos Sci Technol* 2010, **70**: 916–921.

[80] Park JY, Kang SM, Kim WJ, *et al*. Characterization of the SiC_f/SiC composite fabricated by the whisker growing assisted CVI process. *Key Eng Mater* 2005, **287**: 200–205.

[81] Kim WJ, Kang SM, Park JY, *et al*. Effect of a SiC whisker formation on the densification of Tyranno SA/SiC composites fabricated by the CVI process. *Fusion Eng Des* 2006, **81**: 931–936.

[82] Kim WJ, Kang SM, Park JY. Microstructure and properties of SiC nanowire-reinforced SiC_f/SiC composites. *Adv Mater Res* 2009, **59**: 279–282.

[83] Li YJ, Zhang Y, Wang YS. Structure and oxidation behavior of high temperature ZrB_2–SiBCN ceramics with polyborosilazane as a sintering additive. *J Ceram Soc Jpn* 2013, **121**: 520–523.

[84] Guo QG, Song JR, Liu L, *et al*. Relationship between oxidation resistance and structure of B_4C–SiC/C composites with self-healing properties. *Carbon* 1999, **37**: 33–40.

[85] Tang BJ, Feng ZL, Hu SJ, *et al*. Preparation and anti-oxidation characteristics of $ZrSiO_4$–SiBCN(O) amorphous coating. *Appl Surf Sci* 2015, **331**: 490–496.
[86] Shan QL, Feng Q, Hu JB, *et al*. Oxidation behavior in wet oxygen environment of Al_2O_3 added reaction-sintered Si–B–C ceramics. *Ceram Int* 2018, **44**: 4009–4015.
[87] Feng JP, Yan YY, Chen DP, *et al*. Study of thermal stability of fumed silica based thermal insulating composites at high temperatures. *Compos B Eng* 2011, **42**: 1821–1825.
[88] Xie J, Li KZ, Li HJ, *et al*. Ablation behavior and mechanism of C/C–ZrC–SiC composites under an oxyacetylene torch at 3000 ℃. *Ceram Int* 2013, **39**: 4171–4178.
[89] Tan WL, Li KZ, Li HJ, *et al*. Ablation behavior and mechanism of C/C–HfC–SiC composites. *Vacuum* 2015, **116**: 124–129.
[90] Wang YG, Liu W, Cheng LF, *et al*. Preparation and properties of 2D C/ZrB_2–SiC ultra high temperature ceramic composites. *Mater Sci Eng A* 2009, **524**: 129–133.
[91] Feng B, Li HJ, Zhang YL, *et al*. Effect of SiC/ZrC ratio on the mechanical and ablation properties of C/C–SiC–ZrC composites. *Corros Sci* 2014, **82**: 27–35.
[92] Lohfeld S, Schütze M, Böhm A, *et al*. Oxidation behaviour of particle reinforced $MoSi_2$ composites at temperatures up to 1700 ℃. *Mater Corros* 2005, **56**: 250–258.
[93] Ball RGJ, Mignanelli MA, Barry TI, *et al*. The calculation of phase equilibria of oxide core-concrete systems. *J Nucl Mater* 1993, **201**: 238–249.
[94] Shin D, Arróyave R, Liu ZK. Thermodynamic modeling of the Hf–Si–O system. *Calphad* 2006, **30**: 375–386.
[95] Jacobson NS, Lee KN, Fox DS. Reactions of silicon carbide and silicon(IV) oxide at elevated temperatures. *J Am Ceram Soc* 1992, **75**: 1603–1611.
[96] Borisov VG, Yudin BF. Reaction thermodynamics in the SiO_2–SiC system. *Refractories* 1968, **9**: 162–165.
[97] Liu YS, Zhang LT, Cheng LF, *et al*. Preparation and oxidation resistance of 2D C/SiC composites modified by partial boron carbide self-sealing matrix. *Mater Sci Eng A* 2008, **498**: 430–436.
[98] Zuo XZ, Zhang LT, Liu YS, *et al*. Oxidation behaviour of two-dimensional C/SiC modified with self-healing Si–B–C coating in static air. *Corros Sci* 2012, **65**: 87–93.
[99] Liu F, Kong J, Luo CJ, *et al*. High temperature self-healing SiBCN ceramics derived from hyperbranched polyborosilazanes. *Adv Compos Hybrid Mater* 2018, **1**: 506–517.
[100] Xu YD, Cheng LF, Zhang LT, *et al*. Oxidation behavior and mechanical properties of C/SiC composites with Si–$MoSi_2$ oxidation protection coating. *J Mater Sci* 1999, **34**: 6009–6014.
[101] Carney CM, Parthasarathy TA, Cinibulk MK. Oxidation resistance of hafnium diboride ceramics with additions of silicon carbide and tungsten boride or tungsten carbide. *J Am Ceram Soc* 2011, **94**: 2600–2607.
[102] Cheng LF, Xu YD, Zhang LT, *et al*. Effect of glass sealing on the oxidation behavior of three dimensional C/SiC composites in air. *Carbon* 2001, **39**: 1127–1133.
[103] Fan SW, Zhang LT, Cheng LF, *et al*. Preparation and properties of self-healing coating for C/SiC brake materials. *Int J Appl Ceram Technol* 2008, **5**: 204–209.
[104] Isola C, Appendino P, Bosco F, *et al*. Protective glass coating for carbon–carbon composites. *Carbon* 1998, **36**: 1213–1218.
[105] Huang JF, Zhang YL, Zhu KJ, *et al*. Microstructure and oxidation protection of borosilicate glass coating prepared by pulse arc discharge deposition for C/C composites. *Ceram Int* 2015, **41**: 4662–4667.
[106] Liu YS, Men J, Zhang LT, *et al*. Microstructural evolution and self-healing mechanism of a 2D C/SiC–BC_x composite under constant load in static wet oxygen and dynamic combustion atmosphere. *Mater Corros* 2015, **66**: 128–136.
[107] Ye F, Zhang LT, Yin XW, *et al*. Fabrication of Si_3N_4–SiBC composite ceramic and its excellent electromagnetic properties. *J Eur Ceram Soc* 2012, **32**: 4025–4029.
[108] Liu YS, Wan JJ, Zuo XZ, *et al*. Oxidation behavior of 2D C/SiC composites coated with multi-layer SiC/Si–B–C/SiC coatings under wet oxygen atmosphere. *Appl Surf Sci* 2015, **353**: 214–223.
[109] Dong N, Zuo XZ, Liu YS, *et al*. Fatigue behavior of 2D C/SiC composites modified with Si–B–C ceramic in static air. *J Eur Ceram Soc* 2016, **36**: 3691–3696.
[110] Carrère P, Lamon J. Fatigue behavior at high temperature in air of a 2D woven SiC/SiBC with a self healing matrix. *Key Eng Mater* 1998, **164–165**: 321–324.
[111] Forio P, Lamon J. Fatigue behavior at high temperatures in air of a 2D SiC/Si–B–C composite with a self-healing multilayered matrix. In: *Advances in Ceramic Matrix Composites VII*, *Volume 128*. Bansal NP, Singh JP, Lin HT, Eds. Westerville, USA: The American Ceramic Society, 2001: 127–141.
[112] Viricelle JP, Goursat P, Bahloul-Hourlier D. Oxidation behaviour of a multi-layered ceramic-matrix composite $(SiC)_f$/C/$(SiBC)_m$. *Compos Sci Technol* 2001, **61**: 607–614.
[113] Bouillon EP, Spriet PC, Habarou G, *et al*. Engine test and post engine test characterization of self-sealing ceramic matrix composites for nozzle applications in gas turbine engines. In: Proceedings of the ASME Turbo Expo 2004: Power for Land, Sea, and Air, Vienna, Austria, 2008: 409–416.
[114] Christin FA. A global approach to fiber nD architectures and self-sealing matrices: From research to production. *Int J Appl Ceram Technol* 2005, **2**: 97–104.
[115] Bouillon E, Lamouroux F, Baroumes L, *et al*. An improved long life duration CMC for jet aircraft engine applications. In: Proceedings of the ASME Turbo Expo 2002: Power for Land, Sea, and Air, Amsterdam, the Netherlands, 2009: 119–125.
[116] Lamouroux F, Bouillon E, Cavalier JC, *et al*. An improved long life duration CMC for jet aircraft engine applications. In: *High Temperature Ceramic Matrix Composites*. Krenkel W, Naslain R, Schneider H, Eds. Weinheim, Germany: Wiley-VCH Verlag GmbH & Co. KGaA, 2001: 783–788.
[117] Lacombe A, Spriet P, Habarou G, *et al*. Ceramic matrix composites to make breakthroughs in aircraft engine

performance. In: Proceedings of the 50th AIAA/ASME/ASCE/AHS/ASC Structures, Structural Dynamics, and Materials Conference, Palm Springs, USA, 2009: 2009–2675.

[118] Cao XY, Yin XW, Fan XM, *et al*. Effect of PyC interphase thickness on mechanical behaviors of SiBC matrix modified C/SiC composites fabricated by reactive melt infiltration. *Carbon* 2014, **77**: 886–895.

[119] Zhao DL, Fan XM, Yin XW, *et al*. Oxidation behavior of tyranno ZMI–SiC fiber/SiC–SiBC matrix composite from 800 to 1200 ℃. *Materials* 2018, **11**: 1367.

[120] Sun XN, Yin XW, Fan XM, *et al*. Oxidation resistance of SiC/SiC composites containing SiBC matrix fabricated by liquid silicon infiltration. *J Eur Ceram Soc* 2018, **38**: 479–485.

[121] Ma XK, Yin XW, Fan XM, *et al*. Improved tensile strength and toughness of dense C/SiC–SiBC with tailored PyC interphase. *J Eur Ceram Soc* 2019, **39**: 1766–1774.

[122] Zhang PF, Jia DC, Yang ZH, *et al*. Progress of a novel non-oxide Si–B–C–N ceramic and its matrix composites. *J Adv Ceram* 2012, **1**: 157–178.

[123] Wang ZC, Aldinger F, Riedel R. Novel silicon–boron–carbon–nitrogen materials thermally stable up to 2200 ℃. *J Am Ceram Soc* 2001, **84**: 2179–2183.

[124] Baldus HP, Jansen M, Wagner O. New materials in the system Si–(N,C)–B and their characterization. *Key Eng Mater* 1993, **89–91**: 75–80.

[125] Riedel R, Kienzle A, Dressler W, *et al*. A silicoboron carbonitride ceramic stable to 2,000 ℃. *Nature* 1996, **382**: 796–798.

[126] Cinibulk MK, Parthasarathy TA. Characterization of oxidized polymer-derived SiBCN fibers. *J Am Ceram Soc* 2001, **84**: 2197–2202.

[127] Baldus HP, Passing G, Scholz H, *et al*. Properties of amorphous SiBNC-ceramic fibres. *Key Eng Mater* 1996, **127–131**: 177–184.

[128] Zhang CY, Han KQ, Liu Y, *et al*. A novel high yield polyborosilazane precursor for SiBNC ceramic fibers. *Ceram Int* 2017, **43**: 10576–10580.

[129] Rooke MA, Sherwood PMA. Surface studies of potentially oxidation protective Si–B–N–C films for carbon fibers. *Chem Mater* 1997, **9**: 285–296.

[130] Luan XG, Xu XM, Zou Y, *et al*. Wet oxidation behavior of SiC/(SiC–SiBCN)$_x$ composites prepared by CVI combined with PIOP process. *J Am Ceram Soc* 2019, **102**: 6239–6255.

[131] Tan X, Liu W, Cao LM, *et al*. Oxidation behavior of a 2D-SiC$_f$/BN/SiBCN composite at 1350–1650 ℃ in air. *Mater Corros* 2018, **69**: 1227–1236.

[132] Butchereit E, Nickel KG, Müller A. Precursor-derived Si–B–C–N ceramics: Oxidation kinetics. *J Am Ceram Soc* 2001, **84**: 2184–2188.

[133] Lu B, Zhang Y. Oxidation behavior of SiC–SiBCN ceramics. *Ceram Int* 2015, **41**: 1023–1030.

[134] Li DX, Yang ZH, Jia DC, *et al*. Effects of boron addition on the high temperature oxidation resistance of dense sSiBCN monoliths at 1500 ℃. *Corros Sci* 2017, **126**: 10–25.

[135] Liang B, Yang ZH, Jia DC, *et al*. Amorphous silicoboron carbonitride monoliths resistant to flowing air up to 1800 ℃. *Corros Sci* 2016, **109**: 162–173.

[136] Zhang M, Chen QQ, He YP, *et al*. A comparative study on high temperature oxidation behavior of SiC, SiC–BN and SiBCN monoliths. *Corros Sci* 2021, **192**: 109855.

[137] Li DX, Yang ZH, Jia DC, *et al*. High-temperature oxidation behavior of dense SiBCN monoliths: Carbon-content dependent oxidation structure, kinetics and mechanisms. *Corros Sci* 2017, **124**: 103–120.

[138] Luan XG, Xu XM, Wang L, *et al*. Self-healing enhancing tensile creep of 2D-satin weave SiC/(SiC–SiBCN)$_x$ composites in wet oxygen environment. *J Eur Ceram Soc* 2020, **40**: 3509–3519.

[139] Xu HM, Peng YQ, Wei ZH, *et al*. Oxidation behavior of 3D SiC$_f$/SiBCN composites at 800–1200 ℃. *J Eur Ceram Soc* 2021, **41**: 148–157.

[140] Ding Q, Ni DW, Wang Z, *et al*. Mechanical properties and microstructure evolution of 3D C$_f$/SiBCN composites at elevated temperatures. *J Am Ceram Soc* 2018, **101**: 4699–4707.

[141] Butchereit E, Nickel KG. Beneficial effect of Aluminium on the oxidation behvior of precursor-derived ceramics. In: *High Temperature Corrosion and Materials Chemistry IV*. Opila E, Ed. Washington, USA: The Electrochemical Society, 2001: 325–338.

[142] Müller A, Gerstel P, Butchereit E, *et al*. Si/B/C/N/Al precursor-derived ceramics: Synthesis, high temperature behaviour and oxidation resistance. *J Eur Ceram Soc* 2004, **24**: 3409–3417.

[143] Shan QL, Xue YD, Hu JB, *et al*. More effective crack self-healing capability of SiC$_f$/SiC–B$_4$C with Al$_2$O$_3$ modified under wet environment. *J Am Ceram Soc* 2020, **103**: 7247–7258.

[144] Shan QL, Wang QL, Xue YD, *et al*. The surface cracking resistance of Al$_2$O$_3$-modified SiC$_f$/SiC–B$_4$C composites after cyclic oxidation in wet environment. *Adv Eng Mater* 2019, **21**: 1900458.

[145] Miao Y, Yang ZH, Liang B, *et al*. A novel *in situ* synthesis of SiBCN–Zr composites prepared by a sol–gel process and spark plasma sintering. *Dalton Trans* 2016, **45**: 12739–12744.

[146] Miao Y, Yang ZH, Liang B, *et al*. Oxidation behavior of SiBCN–Zr composites at 1500 ℃ prepared by reactive spark plasma sintering. *Corros Sci* 2018, **132**: 293–299.

[147] Miao Y, Yang ZH, Wang WX, *et al*. Microstructure and thermal shock behavior of sol–gel introduced ZrB$_2$ reinforced SiBCN matrix. *J Sol Gel Sci Technol* 2018, **86**: 365–373.

[148] Yao XY, Li HJ, Zhang YL, *et al*. A SiC–Si–ZrB$_2$ multiphase oxidation protective ceramic coating for SiC-coated carbon/carbon composites. *Ceram Int* 2012, **38**: 2095–2100.

[149] Miao Y, Zhang FN, Yang ZH, *et al*. Incorporation of BN-coated carbon fibers into ZrB$_2$/SiBCN ceramic composites and their ablation behavior. *J Eur Ceram Soc* 2020, **40**: 1078–1085.

[150] Li DX, Yang ZH, Jia DC, *et al*. Preparation, microstructures, mechanical properties and oxidation resistance of SiBCN/ZrB_2–ZrN ceramics by reactive hot pressing. *J Eur Ceram Soc* 2015, **35**: 4399–4410.

[151] Kaiser A, Lobert M, Telle R. Thermal stability of zircon ($ZrSiO_4$). *J Eur Ceram Soc* 2008, **28**: 2199–2211.

[152] Ouyang HB, Li CY, Huang JF, *et al*. Self-healing ZrB_2–SiO_2 oxidation resistance coating for SiC coated carbon/carbon composites. *Corros Sci* 2016, **110**: 265–272.

[153] Wang SH, Zhang YC, Sun Y, *et al*. Synthesis and characteristic of SiBCN/HfN ceramics with high temperature oxidation resistance. *J Alloys Compd* 2016, **685**: 828–835.

[154] Luan XG, Zhang JH, Wang L, *et al*. Wet oxidation behavior of C/SiC–SiHf(B)CN composites at high temperature. *Adv Compos Hybrid Mater* 2020, **3**: 415–429.

[155] Verdon C, Szwedek O, Allemand A, *et al*. High temperature oxidation of two- and three-dimensional hafnium carbide and silicon carbide coatings. *J Eur Ceram Soc* 2014, **34**: 879–887.

[156] Wang YJ, Li HJ, Fu QG, *et al*. SiC/HfC/SiC ablation resistant coating for carbon/carbon composites. *Surf Coat Technol* 2012, **206**: 3883–3887.

[157] Huang D, Zhang MY, Huang QZ, *et al*. Mechanical property, oxidation and ablation resistance of C/C–ZrB_2–ZrC–SiC composite fabricated by polymer infiltration and pyrolysis with preform of C_f/ZrB_2. *J Mater Sci Technol* 2017, **33**: 481–486.

[158] Shi XH, Huo JH, Zhu JL, *et al*. Ablation resistance of SiC–ZrC coating prepared by a simple two-step method on carbon fiber reinforced composites. *Corros Sci* 2014, **88**: 49–55.

[159] Jia YJ, Li HJ, Fu QG, *et al*. A ZrC–SiC/ZrC–LaB_6/ZrC multilayer ablation resistance coating for SiC-coated carbon/carbon composites. *Surf Coat Technol* 2017, **309**: 545–553.